

University of Windsor

Scholarship at UWindor

Electronic Theses and Dissertations

Theses, Dissertations, and Major Papers

6-22-2022

Analysis and Improvement of Electrochemical Impedance Spectroscopy

Rohit Sengar
University of Windsor

Follow this and additional works at: <https://scholar.uwindsor.ca/etd>

Recommended Citation

Sengar, Rohit, "Analysis and Improvement of Electrochemical Impedance Spectroscopy" (2022). *Electronic Theses and Dissertations*. 9592.

<https://scholar.uwindsor.ca/etd/9592>

This online database contains the full-text of PhD dissertations and Masters' theses of University of Windsor students from 1954 forward. These documents are made available for personal study and research purposes only, in accordance with the Canadian Copyright Act and the Creative Commons license—CC BY-NC-ND (Attribution, Non-Commercial, No Derivative Works). Under this license, works must always be attributed to the copyright holder (original author), cannot be used for any commercial purposes, and may not be altered. Any other use would require the permission of the copyright holder. Students may inquire about withdrawing their dissertation and/or thesis from this database. For additional inquiries, please contact the repository administrator via email (scholarship@uwindsor.ca) or by telephone at 519-253-3000ext. 3208.

**ANALYSIS AND IMPROVEMENT OF ELECTROCHEMICAL
IMPEDANCE SPECTROSCOPY FOR BATTERY MANAGEMENT
SYSTEMS**

by
Rohit Sengar

A Thesis
Submitted to the Faculty of Graduate Studies
through the Department of Electrical and Computer Engineering
in Partial Fulfilment of the Requirements for
the Degree of Master of Applied Science at the
University of Windsor

Windsor, Ontario, Canada

© 2022 Rohit Sengar

ANALYSIS AND IMPROVEMENT OF ELECTROCHEMICAL IMPEDANCE
SPECTROSCOPY FOR BATTERY MANAGEMENT SYSTEMS

by
Rohit Sengar

APPROVED BY:

S. Das
Department of Civil and Environmental Engineering

A. Hamdi Sakr
Department of Electrical and Computer Engineering

G. Rankin, Co-Advisor
Department of Mechanical, Automotive & Materials Engineering

B. Balasingam, Co-Advisor
Department of Electrical and Computer Engineering

May 24, 2022

Declaration of Co-Authorship / Previous Publication

Co-Authorship

I hereby declare that this thesis incorporates material that is result of joint research, as follows: Chapter 2 of this thesis was co-authored with Marzia Abaspour and professor Balasingam. Chapter 3 of this thesis was co-authored with professor Balasingam who provided supervision and guidance during the research and writing process.

In all cases, the key ideas, primary contributions, data analysis, interpretation, and writing were performed by the author. In all cases, the key ideas, primary contributions, experimental designs, data analysis, interpretation, and writing were performed by me. I am aware of the University of Windsor Senate Policy on Authorship and I certify that I have properly acknowledged the contribution of other researchers to my thesis, and have obtained written permission from each of the co-author(s) to include the above material(s) in my thesis.

Previous Publication

The thesis include 2 journal papers that have been proviously submitted/ yet to submit to journals for publication, as follows:

Thesis chapter	Publication title/full citation	Publication status
1	Sengar, Rohit, Abaspour, Marzia & Balasingam, Balakumar. Battery Parameter Analysis Through Electrochemical Impedance Spectroscopy at Different State of Charge Levels	Under Review
2	Sengar, Rohit, & Balasingam, Balakumar. Electrochemical Impedance Spectroscopy with Reduced Time Signal	Yet to submit

I certify that I have obtained a written permission from the copyright owner(s) to include the above published material(s) in my thesis. I certify that the above material describes work completed during my registration as a graduate student at the University of Windsor.

General

I declare that, to the best of my knowledge, my thesis does not infringe upon anyone's copyright nor violate any proprietary rights and that any ideas, techniques, quotations, or any other material from the work of other people included in my thesis, published or otherwise, are fully acknowledged in accordance with the standard referencing practices. Furthermore, to the extent that I have included copyrighted material that surpasses the bounds of fair dealing within the meaning of the Canada Copyright Act, I certify that I have obtained a written permission from the copyright owner(s) to include such material(s) in my thesis. I declare that this is a true copy of my thesis, including any final revisions, as approved by my thesis committee and the Graduate Studies office, and that this thesis has not been submitted for a higher degree to any other University or Institution.

Abstract

This thesis aims at estimating the parameters of a battery equivalent circuit model (ECM) using electrochemical impedance spectroscopy (EIS). This method has been widely used for analysing state of health of batteries. However, much work hasn't been done to extract battery ECM parameters using EIS. In this thesis, an approach is offered as a method for obtaining the ECM parameters of a battery using EIS. Also, another approach based on estimation in time domain is developed to estimate the internal resistance of the battery. Further, real world EIS and time-domain data are collected to estimate and compare the ECM parameters using both methods. The experiment is repeated at six different state of charge (SOC) levels of the battery. The analysis showed that at low SOC levels, the experimental results demonstrate a strong solid electrolyte interface (SEI) effect. Furthermore, the experimental data demonstrates that computed ECM parameters using the time-domain technique are very close to those estimated in the frequency domain using EIS data, with a difference of less than 0.01 percent. One major issue that restricts EIS from implementation in real time scenarios is that it is time consuming . EIS experiment takes about 60 minutes to complete. This thesis presents an approach to reduce the EIS data collection time by constructing a new signal where multiple sinewaves are combined to shorten the current signals. This work is done in the simulated environment which showed that shortening the signal increased noise in the output. The algorithms were applied on several signal to noise ratio (SNR) values. Furthermore, simulations demonstrated that at a SNR of 70 EIS time can be reduced to approx. 150 secs.

Acknowledgements

First of all, I would like to express my profound gratitude to my parents, who have blessed me with my existence and the prosperous future in every aspects of my life. Further, I would like to extend my earnest gratitude to my supervisors Dr. B. Balasingam and Dr. G. Rankin who offered me an opportunity to be a graduate student and conduct research under their guidance. He gave me all the support and confidence needed to complete this thesis. I would also like to thank him for spending limitless time in discussing about the research papers, projects and the thesis.

I would also like to thank all the staff members of our department for their kind support. Especially, I thank Andria Ballo for her help and support. Further I thank the fellow graduate students for their cooperation during the research period.

Contents

Declaration of Co-Authorship / Previous Publication	iii
Abstract	v
Acknowledgements	vi
List of Figures	ix
1 Introduction	1
1.1 Organization of the Thesis	3
2 Battery Parameter Analysis Through Electrochemical Impedance Spectroscopy at Different State of Charge Levels	5
2.1 Introduction	5
2.2 Frequency Domain Approach to ECM Parameter Estimation	7
2.2.1 Estimation of Ohmic Resistance and Stray Inductance	10
2.2.2 Estimation of Warburg Coefficient	10
2.2.3 Estimation of R_{CT} and C_{DL}	11
2.2.4 Estimation of R_{SEI} and C_{SEI}	12
2.3 Time Domain Approach to ECM Parameter Estimation	14
2.4 Experimental Procedure	16
2.5 Results	18
2.6 Conclusion	39

2.7	References	40
3	Electrochemical Impedance Spectroscopy with Reduced Time Signal	44
3.1	Introduction	44
3.2	Construction of Perturbation Current Signal	46
3.3	Obtaining the Nyquist Plots	49
3.4	Results	50
3.5	Conclusion	51
3.6	References	63
4	Conclusion and Future Work	66
	Vita Auctoris	68

List of Figures

2.1	Adaptive Randles ECM model.	8
2.2	Nyquist plot	9
2.3	Discharge current stairs.	14
2.4	Voltage across a simple resistor	15
2.5	Experimental details. EIS and staircase signals are applied at different SOC levels (Circle details the applied current profile)	17
2.6	Experimental procedure.	19
2.7	Nyquist plots for B3201	20
2.8	Nyquist plots for B3202	21
2.9	Nyquist plots for B3203	22
2.10	Estimated parameter values	23
2.11	Estimated paramters for B3201 (Inductance and Warburg coefficient)	24
2.12	Estimated paramters for B3202 (Inductance and Warburg coefficient)	25
2.13	Estimated paramters for B3203 (Inductance and Warburg coefficient)	26
2.14	Estimated paramters for B3201 (Resistances)	27
2.15	Estimated paramters for B3202 (Resistances)	28
2.16	Estimated paramters for B3203 (Resistances)	29
2.17	Estimated paramters for B3201 (Capacitances)	30

2.18	Estimated paramters for B3202 (Capacitances)	31
2.19	Estimated paramters for B3203 (Capacitances)	32
2.20	Estimated paramters for B3201 (Resistances in time domain and frequency domain)	33
2.21	Estimated paramters for B3202 (Resistances in time domain and frequency domain)	34
2.22	Estimated paramters for B3203 (Resistances in time domain and frequency domain)	35
2.23	Percentage difference between time-domain and frequency do- main estimates (B3201)	36
2.24	Percentage difference between time-domain and frequency do- main estimates (B3202)	37
2.25	Percentage difference between time-domain and frequency do- main estimates (B3203)	38
3.26	Sine wave with $n = 2$ (Since $n = 2$ each sine wave is constructed using 5 frequencies)	48
3.27	Sine wave with $n = 2$	49
3.28	Current signal for (a) $n = 2$, (b) $n = 4$, (c) $n = 6$	52
3.29	Nyquist plots for $n = 2$	53
3.30	Nyquist plots for $n = 4$	54
3.31	Nyquist plots for $n = 6$	55
3.32	Estimated ohmic resistance for different n	56
3.33	Estimated stray inductance for different n	57
3.34	Estimated Warburg impedance for different n	58
3.35	Estimated charge transfer resistance for different n	59
3.36	Estimated double layer capacitance for different n	60
3.37	Estimated solid electrolytic interface resistance for different n	61
3.38	Estimated solid electrolytic interface capacitance for different n	62

Chapter 1

Introduction

In this manuscript style thesis, we aim at the research in the field of battery management systems (BMS) through a collection of previously submitted works. As the world is growing towards technology, the demand for energy is also increasing. Due to environmental concerns of the fossil fuels, the need for renewable energy resources comes into play. Li-ion battery has been widely used in variety of fields because of their high energy density and low memory effect. A battery management system plays a vital role in ensuring the safety, reliability and efficiency of the battery. The evolution of the battery management system (BMS) from a simple monitoring unit to a multifunction integrated unit is being accelerated by advancements in battery technology. It would be more accurate and effective to represent the behaviour of the battery level to the vehicle with a more comprehensive and faster battery model. Some essential technologies based on the model, such as battery condition estimate, energy equalisation, thermal management, and fault diagnosis, are progressed on this premise to ensure battery safety, power, and durability. For the deployment of effective BMS control, a battery model must be established. A battery model is the behaviour of a battery in terms of its electrical equivalent circuit model (ECM). The accuracy in estimating parameters of electrical ECM is directly related to the efficiency of BMS. BMS comprises of three major components, named as optimal

charging algorithms (OCA), cell balancing circuitry (CBC), and battery fuel gauge (BFG). Optimal charging algorithms focus on the charging strategies, charging current, charging rate, keeping the voltage in safe limits. Moreover, each cell of the battery might not behave the same way. So, there is a possibility that battery state of charge (SOC) won't be balanced. CBC takes charge from one cell and transfers it to others unless their SOC becomes equal. BFG determines the current state of the battery, available power inside the battery. OCA and CBC can perform efficiently only if BFG is performing efficiently. The accuracy of BFG depends on the ECM model used and accuracy in estimating parameters of the battery.

There are two methods to estimate parameters of battery, time domain and frequency domain. Though parameter estimation in time domain is more suitable for real time application. Parameter estimation in frequency domain performs better in tracing battery characteristics. Electrochemical impedance spectroscopy (EIS) is a widely used technique to characterize electrical and electrochemical behaviour of batteries. This technique depicts the impedance response of the battery in terms of Nyquist plot. This impedance response of the battery can be used to characterize its ECM and parameters can be estimated.

The thesis is focused on parameter estimation of the battery electrical ECM model through frequency domain methods. We use adaptive Randles ECM model and estimate the parameters of a real battery. In the literature, little has been done to estimate ECM parameters using multiple measurements. Moreover, little has been done to estimate parameters of a real battery. Comparison of time domain and frequency domain methods for a real battery hasn't been extensively explored yet in the literature. Therefore, we focus on estimating parameters for a real battery in the frequency domain and make a comparison with time domain. ECM parameter algorithms use least square estimation technique with multiple measurements. The time taken by EIS to obtain an impedance response of the battery is significantly large to be implemented real time. Therefore, we further propose a method to reduce

the time taken by EIS to obtain an impedance response of the battery and estimate its ECM parameters in a simulated environment.

1.1 Organization of the Thesis

This thesis is presented in a manuscript format. That is, the chapters that follow are made up of manuscripts that are written or submitted as first author. The manuscript chapters 2, and 3, (referred to as "manuscript chapters" herein) are included in this thesis as prepared at the time of their submissions, in chronological sequence, with minor changes to format and content to preserve a cohesive thesis framework. Abstracts were likewise omitted, as required by the manuscript format. The author believes that the selected style appropriately conveys their thought process, knowledge of the research issue and its role in the current world, and journey toward creating increasingly relevant contributions.

While a standard thesis would typically include a general literature review and a problem statement, we have chosen to omit these elements. The reader will notice that each manuscript chapter has its own introduction, which serves to familiarise the reader with the study environment as well as relevant literature. The inclusion of a general literature review and a problem statement in this thesis would be redundant. It should be noted, because the book chapters were originally written as separate, autonomous entities, there might be some redundancy across them.

The remainder of this thesis is organized as follows:- In Chapter 2, the first of the author's work is presented. This is an experimental work. In this chapter, parameter estimation algorithm using least square estimation technique using multiple measurements are tested using real world data. The results are then compared with time domain parameter estimation and errors are plotted. The data is collected for 3 Samsung batteries of the same kind. The experiment is performed on an Arbin battery cycler (time domain data collection) and Gamry interface 5000P EIS device. However,

time taken by the EIS is significantly large to be implemented real time. Chapter 3 focuses on this problem. In Chapter 3, we propose a new current signal which require less time to perform the EIS of a Li-ion battery. Chapter 3 is a simulation work where EIS data provided by Gamry EIS device is extracted using simulation. The algorithms in Chapter 2 are applied to this data and the parameters are estimated. Since it is a simulation work, the errors in parameter estimation at different signal length is plotted against signal to noise ratio (SNR).

Chapter 2

Battery Parameter Analysis Through Electrochemical Impedance Spectroscopy at Different State of Charge Levels

2.1 Introduction

Batteries are crucial energy storage systems and lithium based rechargeable battery packs have been widely adopted in electric vehicles (EVs). Behaviour of Li-ion battery is highly non-linear. A battery management system (BMS) [1] ensures the safety, efficiency and reliability of the electric vehicle by continuously monitoring the battery packs. The main component of a BMS is the battery fuel gauge (BFG). The BFG estimates all the critical parameters of the battery, such as, state of charge (SOC), state of health (SOH), time to shut down (TTS) and remaining useful life (RUL) [2–4]. In order for the BFG to achieve all these aspects, identifying a battery model and estimating its parameters remains a crucial step [5].

Two approaches have been developed so far in the literature for estimating battery

electrical ECM parameters: time domain and frequency domain approaches [6]. In the time domain approach, voltage and current measurements from the battery are used [7, 8] to estimate ECM Parameters.

Electrochemical impedance spectroscopy (EIS) is a well known frequency domain technique which outputs the impedance in frequency response of the battery [9]. It was introduced by Heaviside in 1894 [10]. In EIS, specially excited signals with varying frequency are superimposed on the charging or discharging current to the battery. The measured time domain responses (voltage and current) are converted to frequency domain using fast Fourier transform [11] and the impedance is computed in the frequency domain. The battery equivalent model parameters can be estimated based on the impedance computed at specified range of frequencies.

Significant work has been reported in the literature using the EIS technique. A precise impedance measurement technique with offset clipping and amplifying signals together with FFT along with computing peak amplitudes and phase difference estimations [9]. Physics based battery modelling using EIS technique has been done [12]. Non-linear least square estimation techniques are also used [13] to estimate the ECM parameters of the battery. Support vector machines (SVM) have been used [13] to estimate and track the SOC and SOH of the battery. Fractional order models have also been developed using EIS technique for estimation of SOC of the battery [14]. Another fractional order impedance model for lithium-ion batteries using EIS was developed in [15]. Battery aging identification and quantification was done using EIS for four parallel Li-ion cells [16]. A power converter was used with closed loop for step perturbation current for better control of the output [17] from EIS. Non linear least square techniques to estimate battery ECM parameters in the presence of Gaussian noise with high signal-to-noise ratio (SNR) has also been employed [18]. A circuit parameter extraction algorithm for LIB charging system using online EIS was used [19]. In [20], parameter estimation in time domain and frequency domain is done.

EIS at different SOC levels is performed [15, 20–22]. However, time domain parameter estimation was not done at different SOC levels [20]. Accuracy of results was not shown [21]. Least square genetic algorithm(LSGA) were also used [15]. However, resulting parameters at different SOC were not shown [15]. EIS at different SOC levels was also performed by [22]. However, the authors did the experiment for seeking the effect in SOH and didn't show the results of parameters estimated.

In this paper, battery parameters are estimated by collecting EIS data in frequency domain at different levels of SOC and time domain using a staircase current profile. The experiment is designed in such a way that frequency domain and time domain profiles are obtained at 100%, 80%, 60%, 40%, 20% and 0% SOC during slow discharge and charge of the battery. The paper contributes the following: (i) Least Square estimation technique to develop improved algorithms for battery ECM parameter estimation using multiple measurements to remove the effect of noise in the frequency domain, (ii) improved time domain parameter estimation technique using multiple measurements to remove the effect of noise, (iii) Implementation of algorithms at real battery data using Hardware in loop (HIL) and (iv) comparison between time domain and frequency domain parameter estimation to validate the results

The remainder of the paper is organised as follows, Section II describes the algorithms used to estimate ECM parameters in the frequency domain. Section III describes the algorithms to estimate ECM parameters in the time domain. The experimental procedure is explained in section IV. Results are discussed in section V. Section VI concludes the paper.

2.2 Frequency Domain Approach to ECM Parameter Estimation

EIS is a widely used technique to study the impedance response of the battery. In EIS, a small perturbation current over a wide range of frequency (0.01 Hz to 10kHz)

is supplied to the battery and its impedance at those frequencies is measured. Afterwards, a Nyquist plot is generated which has real values of impedance on the X-axis and imaginary values on the Y-axis [23,24].

The frequency domain approach uses the adaptive Randles ECM. The adaptive Randles ECM consists of the following elements: battery voltage source, ohmic resistance (R), stray inductance (L), resistance due to SEI layer (R_{SEI}), capacitance due to SEI layer (C_{SEI}), charge transfer resistance (R_{CT}), double layer capacitance (C_{DL}) and Warburg impedance (Z_w)

Figure 2.1 shows the adaptive Randles ECM model. In Figure 2.2, a Nyquist plot in relation to Figure 2.1 is shown.

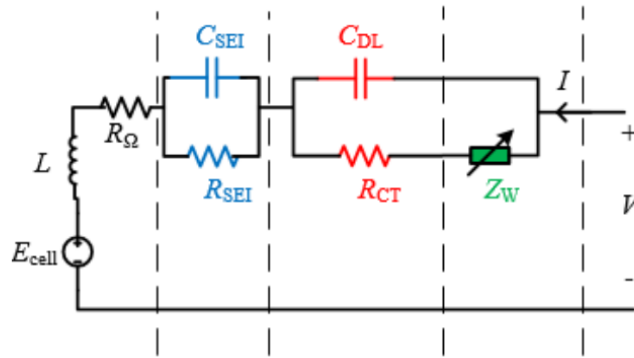


Figure 2.1: **Adaptive Randles ECM model.**

In the Figure 2.2 the points $k_1, k_{2l}, k_{2h}, k_{3l}, k_{3h}$ and k_4 are termed as feature points. Features points are points in the Nyquist plot data. Since, Figure 2.1 and 2.2 clearly indicate that adaptive Randles model is directly related to Nyquist plot, it needs to be divided into sections. These sections are impedance values corresponding to the frequency values in the curve.

- k_1 is selected such that $0 - k_1$ follows the linear line.
- k_{2l} is selected in the middle of the CT arc intuitively, such that it starts to follow the arc.

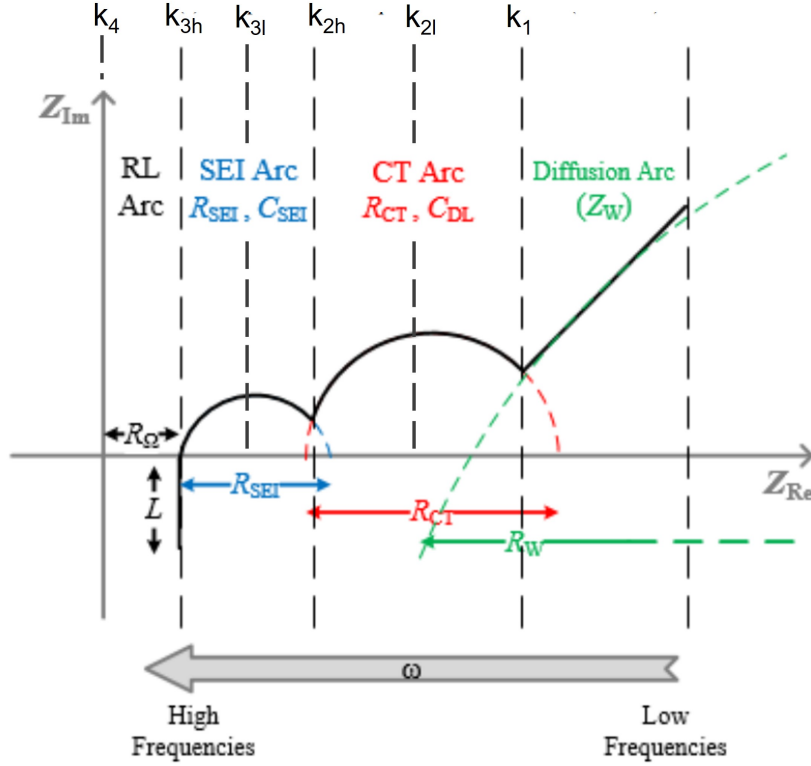


Figure 2.2: Nyquist plot

- k_{2h} is selected at the end of CT arc, such that k_{2l} to k_{2h} follows the arc with the best fit.
- Similarly, k_{3l} is selected in the middle of the SEI arc intuitively.
- k_{3h} is selected at the end of CT arc, such that k_{2l} to k_{3h} fits best to the CT arc.

The parameter estimation algorithms used in the paper uses the basic concept of RC effect, where the effect of C is visible in the imaginary part of impedance and effect of R is seen in the real part of the impedance. The parameter estimation using Nyquist plot is a curve fitting problem which is solved using least square estimation to reduce the effect of measurement noise. In the remainder of this section the parameter estimation approach [25] is summarized.

2.2.1 Estimation of Ohmic Resistance and Stray Inductance

As stated in [25], ohmic resistance and stray inductance can be estimated as:

$$\hat{R}_\Omega = \frac{1}{k_4 - k_{3h}} \sum_{k=k_{3h}+1}^{k_4} Z_r(k) \quad (2.1)$$

$$\hat{L} = \frac{1}{k_4 - k_{3h}} \sum_{k=k_{3h}+1}^{k_4} Z_i(k) \quad (2.2)$$

2.2.2 Estimation of Warburg Coefficient

Warburg impedance is defined mathematically as :

$$Z_w(j\omega) = (1 - j) \frac{\sigma}{\sqrt{\omega}} \quad (2.3)$$

where σ is called as the Warburg coefficient.

From the figure 2.2, it is clear that Warburg impedance is significant only at lower frequencies ($(\omega < \omega_{k_1})$)

Taking real part of Z upto k_1 .

$$\begin{aligned} \mathbf{z} &= \mathbf{b}\sigma \\ Z_r(0) - Z_r(k_1) &= \left(\frac{1}{\sqrt{\omega_0}} - \frac{1}{\sqrt{\omega_{k_1}}} \right) \sigma \\ Z_r(1) - Z_r(k_1 - 1) &= \left(\frac{1}{\sqrt{\omega_1}} - \frac{1}{\sqrt{\omega_{k_1-1}}} \right) \sigma \\ &\vdots \\ Z_r(n) - Z_r(k_1 - n) &= \left(\frac{1}{\sqrt{\omega_n}} - \frac{1}{\sqrt{\omega_{k_1-n}}} \right) \sigma \end{aligned} \quad (2.4)$$

where $n < k_1/2$

The equations in (2.4) can be written with noise model in the form

$$\mathbf{z} = \mathbf{b}\sigma + \mathbf{n} \quad (2.5)$$

So, the least square estimate of σ is

$$\hat{\sigma} = (\mathbf{b}^T \mathbf{b})^{-1} (\mathbf{b}^T \mathbf{z}) \quad (2.6)$$

2.2.3 Estimation of R_{CT} and C_{DL}

The effect of CT arc can be seen in frequencies ($\omega_{k_{2l}} \leq \omega \leq \omega_{k_{2h}}$).

$$Z_F(\omega) = \frac{1}{\frac{1}{R_{CT} + Z_w(j\omega)} + j\omega C_{DL}} \quad (2.7)$$

The R_{CT} and C_{DL} can be estimated by fitting a circle. Assuming the centre of circle lies on the real axis, the equation of a circle at an offset from the origin is given by:

$$\begin{aligned} Z_r^2 + Z_i^2 + aZ_r + b &= 0 \\ \left(Z_r + \frac{a}{2}\right)^2 + Z_i^2 &= \frac{a^2}{4} - b \end{aligned} \quad (2.8)$$

In order to find values of a and b , equation (2.8) can be written using values of Z_r and Z_i from k_1 to k_2 in the matrix form as:

$$\underbrace{\begin{bmatrix} -(Z_r(k_{2l} + 1))^2 + Z_i(k_{2l} + 1)^2 \\ -(Z_r(k_{2l} + 2))^2 + Z_i(k_{2l} + 2)^2 \\ \vdots \\ -(Z_r(k_2))^2 + Z_i(k_{2h})^2 \end{bmatrix}}_{\mathbf{z}} = \underbrace{\begin{bmatrix} Z_r(k_{2l} + 1) & 1 \\ Z_r(k_{2l} + 2) & 1 \\ \vdots & \vdots \\ Z_r(k_{2l}) & 1 \end{bmatrix}}_{\mathbf{B}} \underbrace{\begin{bmatrix} a \\ b \end{bmatrix}}_{\mathbf{x}} + \underbrace{\begin{bmatrix} n_v(1) \\ n_v(2) \\ \vdots \\ n_v(n) \end{bmatrix}}_{\mathbf{n}} \quad (2.9)$$

From equation (2.9) values of a and b can be estimated using least squares as

$$\hat{\mathbf{x}} = (\mathbf{B}^T \mathbf{B})^{-1} (\mathbf{B}^T \mathbf{z}) \quad (2.10)$$

After substituting values of a and b from $\hat{\mathbf{x}}$, R_{CT} can be calculated using equation (2.8) as:

$$\hat{R}_{CT} = 2\sqrt{\frac{a^2}{4} - b} \quad (2.11)$$

The inverse of equation (2.7) can be written as

$$\text{Im} \left(\frac{1}{Z_F(\omega)} \right) = \frac{\frac{\sigma}{\sqrt{\omega}}}{\left(R_{CT} + \frac{\sigma}{\sqrt{\omega}} \right)^2 + \frac{\sigma^2}{\omega}} + \omega C_{DL} \quad (2.12)$$

Substituting values of R_{CT} in equation (2.12) at $\omega = \omega_k$,

$$\tilde{C}_{DL} = \frac{1}{\omega_k} \left(\text{Im} \frac{1}{Z_F(\omega_k)} - \frac{\frac{\sigma}{\sqrt{\omega_k}}}{\left(\hat{R}_{CT} + \frac{\sigma}{\sqrt{\omega_k}} \right)^2 + \frac{\sigma^2}{\omega_k}} \right) \quad (2.13)$$

Afterwards, C_{DL} can be estimated by averaging all values of \tilde{C}_{DL} from equation (2.13) as

$$\hat{C}_{DL} = \frac{1}{k_{2h} - k_{2l}} \sum_{k=k_{2l}+1}^{k_{2h}} \tilde{C}_{DL}(k) \quad (2.14)$$

2.2.4 Estimation of R_{SEI} and C_{SEI}

A similar process for estimation of R_{CT} and C_{DL} is used to estimate R_{SEI} and C_{SEI} . The equation of impedance for frequencies ($\omega_{k_{3l}} \leq \omega \leq \omega_{k_{3h}}$) including the R_{SEI} and C_{SEI}

as:

$$Z_{\text{SEI}} = \frac{1}{\frac{1}{R_{\text{SEI}}} + j\omega C_{\text{SEI}}} \quad (2.15)$$

Estimation of SEI components is also a curve fitting problem of a circular equation. Therefore, the equation of a circle having the centre at some distance from the origin is given by

$$\begin{aligned} Z_r^2 + Z_i^2 + cZ_r + d &= 0 \\ \left(Z_r + \frac{c}{2}\right)^2 + Z_i^2 &= \frac{c^2}{4} - d \end{aligned} \quad (2.16)$$

Now, (2.16) can be written in the matrix form as

$$\underbrace{\begin{bmatrix} -(Z_r(k_{3l} + 1))^2 + Z_i(k_{3l} + 1)^2 \\ -(Z_r(k_{3l} + 2))^2 + Z_i(k_{3l} + 2)^2 \\ \vdots \\ -(Z_r(k_{3h}))^2 + Z_i(k_{3h})^2 \end{bmatrix}}_{\mathbf{z}} = \underbrace{\begin{bmatrix} Z_r(k_{3l} + 1) & 1 \\ Z_r(k_{3l} + 2) & 1 \\ \vdots \\ Z_r(k_{3l}) & 1 \end{bmatrix}}_{\mathbf{B}} \underbrace{\begin{bmatrix} c \\ d \end{bmatrix}}_{\mathbf{y}} + \underbrace{\begin{bmatrix} n_v(1) \\ n_v(2) \\ \vdots \\ n_v(n) \end{bmatrix}}_{\mathbf{n}} \quad (2.17)$$

Hence, using least square estimated values of c and d are

$$\hat{\mathbf{y}} = (\mathbf{B}^T \mathbf{B})^{-1} (\mathbf{B}^T \mathbf{z}) \quad (2.18)$$

Now, substituting the values of c and d in equation (2.16) R_{SEI} can be calculated as

$$\hat{R}_{\text{SEI}} = 2\sqrt{\frac{c^2}{4} - d} \quad (2.19)$$

To estimate the value of C_{SEI} inverse of equation (2.15) can be written as

$$\frac{1}{Z_{\text{SEI}}} = \frac{1}{R_{\text{SEI}}} + j\omega C_{\text{SEI}} \quad (2.20)$$

Substituting the value of R_{CT} from (2.19) in equation (2.20) , C_{SEI} can be estimated as

$$\tilde{C}_{SEI} = \left(\frac{1}{\omega_k} \right) \text{Im} \left(\frac{1}{Z_{SEI}(\omega_k)} \right) \quad (2.21)$$

Finally, all the values of C_{SEI} from equation (2.21) are averaged .

$$\hat{C}_{SEI} = \frac{1}{k_{3h} - k_{3l}} \sum_{k=k_{3l}+1}^{k_{3h}} \tilde{C}_{SEI}(k) \quad (2.22)$$

2.3 Time Domain Approach to ECM Parameter Estimation

Time domain approaches are widely used in the literature to estimate the internal resistance of the battery. Due to less time consumption of experimentation they are more suitable for real time applications [7, 8, 23]. The most well known method to estimate the internal resistance of the battery is the staircase current profile. This method incorporates the charging or discharging at very short periods in the structure of a stair as shown in Fig 2.3.

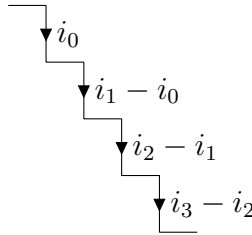


Figure 2.3: Discharge current stairs.

Figure 2.4 shows the battery equivalent circuit model for time domain approach. Since, in staircase method, DC current stairs are applied to the battery, only internal resistance R_0 of the battery can be estimated.

When a current $i(k)$ is supplied to the battery, the voltage across terminal $z_v(k)$

is measured. $z_v(k)$ can be written as

$$z_v(k) = E + i(k)R_0 \quad (2.23)$$

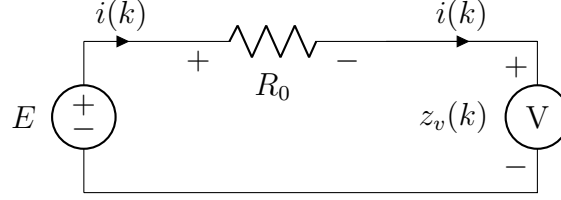


Figure 2.4: **Voltage across a simple resistor**

In the presence of measurement noise from the voltage sensor, the equation (2.23) can be rewritten as

$$z_v(k) = E + i(k)R_0 + n_v(k) \quad (2.24)$$

Considering n measurements of the voltage (stairs), equation (2.24) can be written as

$$\begin{aligned} z_v(1) &= E + i(1)R_0 + n_v(1) \\ &\vdots \\ z_v(n) &= E + i(n)R_0 + n_v(n) \end{aligned} \quad (2.25)$$

The equation (2.25) can be written in the matrix form as

$$\underbrace{\begin{bmatrix} z_v(1) \\ z_v(2) \\ \vdots \\ z_v(n) \end{bmatrix}}_{\mathbf{z}} = \underbrace{\begin{bmatrix} 1 & i(1) \\ 1 & i(2) \\ \vdots & \vdots \\ 1 & i(n) \end{bmatrix}}_{\mathbf{P}} \underbrace{\begin{bmatrix} E & R_0 \end{bmatrix}}_{\mathbf{k}} + \underbrace{\begin{bmatrix} n_v(1) \\ n_v(2) \\ \vdots \\ n_v(n) \end{bmatrix}}_{\mathbf{n}} \quad (2.26)$$

Now, R_0 and E can be estimated using least square approach as

$$\hat{\mathbf{k}} = (\mathbf{P}^T \mathbf{P})^{-1} (\mathbf{P}^T \mathbf{z}) \quad (2.27)$$

2.4 Experimental Procedure

In this section, the experimental procedure is explained. Each experiment started with a fully charged battery (SOC = 100 %) and the SOC is reduced by 20% increments until the SOC reached 0%. After that, the SOC is increased 20% at each time until the SOC reached back to 100%. In summary, the battery SOC is changed to 100%, 80%, 60%, 40%, 20%, 0%, 20%, 40%, 60%, 80%, and 100%. At each of these SOC levels, an EIS experiment is performed, along with a time-domain experiment by applying the staircase waveform. In order to estimate the time domain parameters, a staircase signal detailed in Section 2.3 is applied right after the time EIS experiment at each SOC level.

Figure 2.5 shows the instances of EIS and staircase signals at the above mentioned SOC levels for the battery. When the SOC is 100%, the EIS and staircase signals are applied only in the discharging direction. When the SOC is in the mid range (80% to 40%), the EIS and staircase signals are applied in both charging and discharging directions; and when the SOC is in the lower range (20% and 0%), the EIS and staircase signals are applied only in the discharging direction. The experiment is repeated for three batteries of the same type.

The experimental procedure used to create the voltage-current profile shown in Figure 2.5 consists of the following operations:

- **Fully charge the battery**
 - Measure rest voltage v across the battery terminals
 - If $v < V_{\text{nom}}$ (3.7) (Nominal Voltage), constant current (CC) charge with $C/10$ ($\frac{\text{Battery capacity}}{10}$ A) until terminal voltage reached OCV_{max}

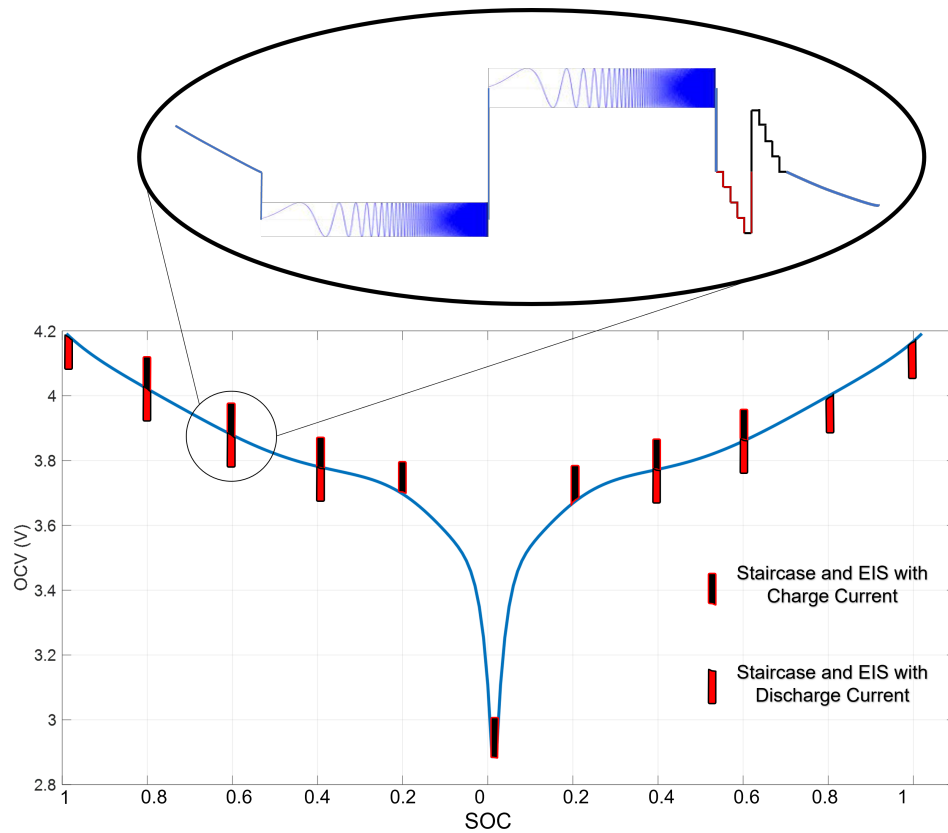


Figure 2.5: **Experimental details.** EIS and staircase signals are applied at different SOC levels (Circle details the applied current profile)

* Switch to CV-charge until current falls below 10mA

– If $v > V_{nom}$, do constant voltage (CV) at OCV_{max} directly until $i < 10mA$

- **EIS test with charge/discharge current**

– Apply 200mA charge/discharge DC with 50 mA sinusoid superimposed on it.

– Frequency range (0.01Hz to 10kHz)

– Duration of EIS is 1 hour approximate

- **Compensate for the SOC gained/lost during EIS test**

– Charge/discharge with 200 mA for 1 hour (sampling 1 Hz) or until voltage reaches OCV_{max} or OCV_{min}

- **Increase/reduce SOC by 20% (sampling rate: 1Hz)**
 - Apply 200mA charge/discharge for 3.5 hours
- **Staircase profile (charge/discharge) (sampling rate: 200 Hz)**
 - Rest for 25ms
 - 40, 80, 120, 160mA charge/discharge for 25 ms each.
 - Rest for 25 ms
- **Bring SOC to 100% or 0%.** Apply a constant charge/discharge current of $C/20$ until the voltage reached OCV_{\max}/OCV_{\min} .

The experimental setup is shown in Figure 2.6 (b) is used to collect data from three of LG INR18650 MJ1 Li-ion batteries by applying the experimental procedure detailed in Section 2.4. These batteries have a nominal voltage of 3.7V with a nominal capacity of 3500 mAh. They are labelled as B3201, B3202, and B3203. The experimental data is collected using the Arbin battery cycler shown in Figure 2.6 (b). The Arbin cycler has 16 channels that can operate in parallel; three channels were used to collect the data simultaneously at room temperature. The EIS data is collected by the Arbin system using a Gamry interface 5000P EIS Device. Gamry EIS device and Arbin battery cycler are operated using the software named Mits Pro provided by Arbin.

2.5 Results

In this section results obtained from the experiment are shown and discussed.

The Nyquist plots at different SOC levels are shown in Figure 2.7, 3.29 and 2.9. The algorithms explained in Section 2.2 are applied to the data in Figures 2.7, 3.29 and 2.9 and ECM parameters are estimated. From Figure 2.7, 3.29 and 2.9, it can be noticed that SEI layer can be seen in only one Nyquist plot for a battery, i.e., the SEI effect is observed at zero SOC.

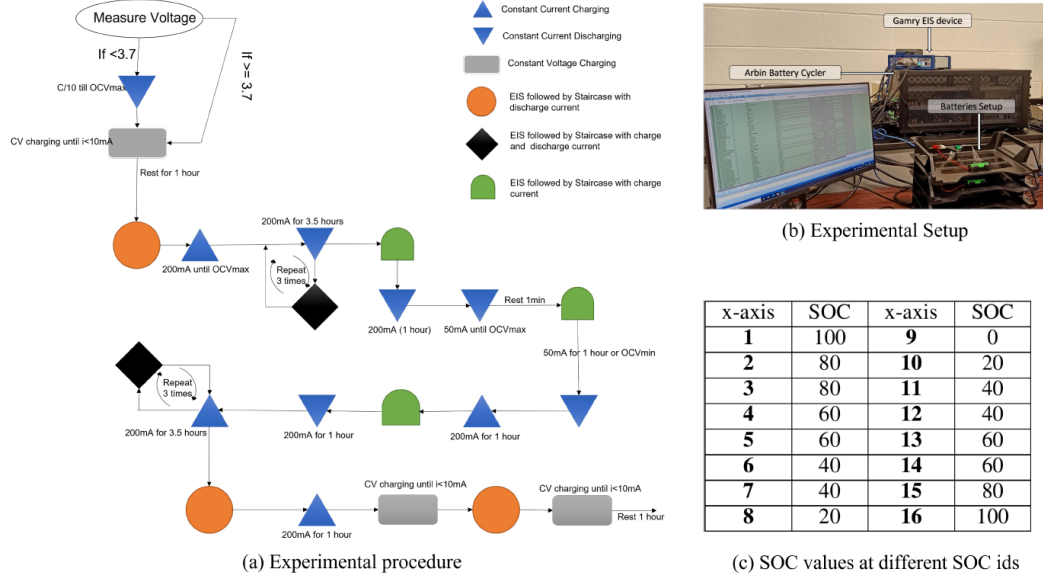


Figure 2.6: **Experimental procedure.**

Figure 2.10 shows all the estimated ECM parameters using the frequency-domain and time-domain approaches presented in Section 2.2 and Section 2.3, respectively. These parameters are also presented as plots in Figure 2.11 to Figure 2.22. The x-axis in each plot refer to the sequence in which the battery was discharged first and then charged, as shown in Figure 2.5. The numbers 1, 2, 3, 4, 5, 6, 7, 8, 9, 10, 11, 12, 13, 14, 15, and 16, on the x-axis denote the SOC values 100, 80, 80, 60, 60, 40, 40, 20, 0, 20, 40, 40, 60, 60, 80, and 100, respectively. Figure 2.6 (c) shows the SOC Ids corresponding to the SOC of the battery.

Figure 2.11 to Figure 2.22 correspond to estimated parameters for batteries B3201, B3202, and B3203. Since R_0 represents all the resistive elements in the battery, it is compared with $R_{CT} + R_{\Omega} + R_{SEI}$. Figure 2.23 to Figure 2.25 shows the percentage difference between R_0 and $R_{CT} + R_{\Omega} + R_{SEI}$. It can be seen that the difference is in fractions of a percentage at all SOC levels.

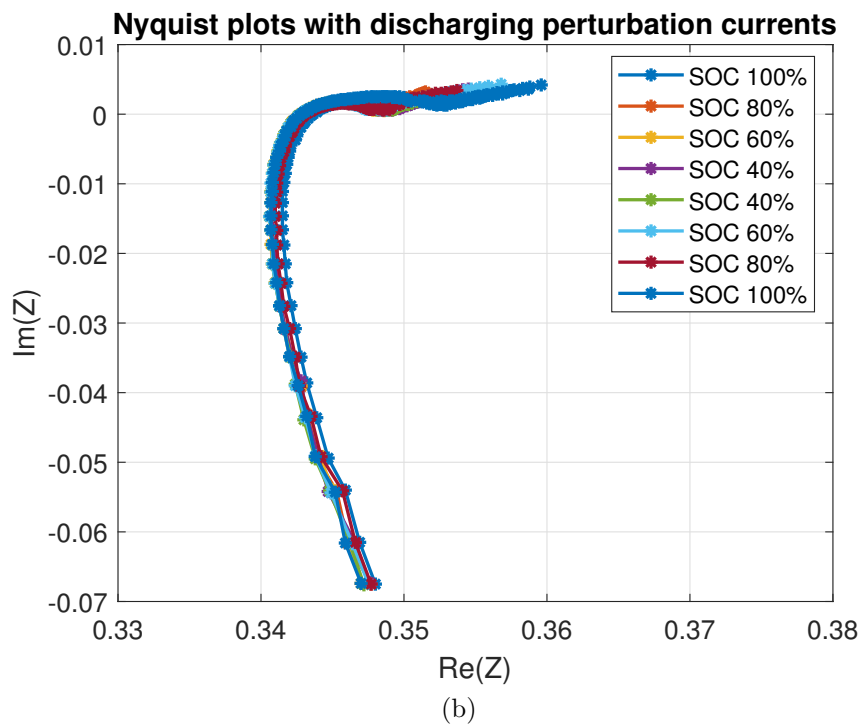
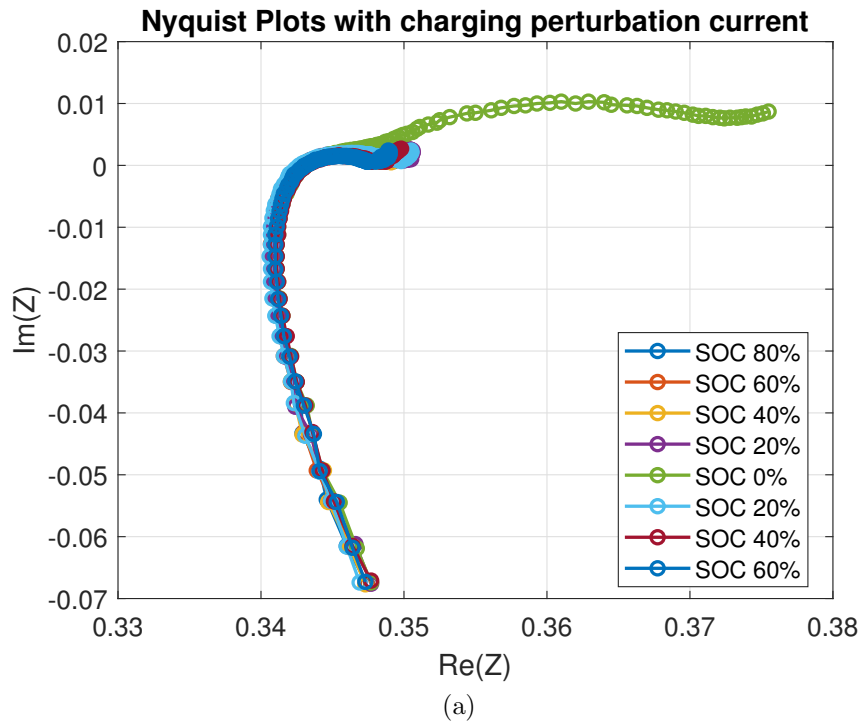


Figure 2.7: Nyquist plots for B3201

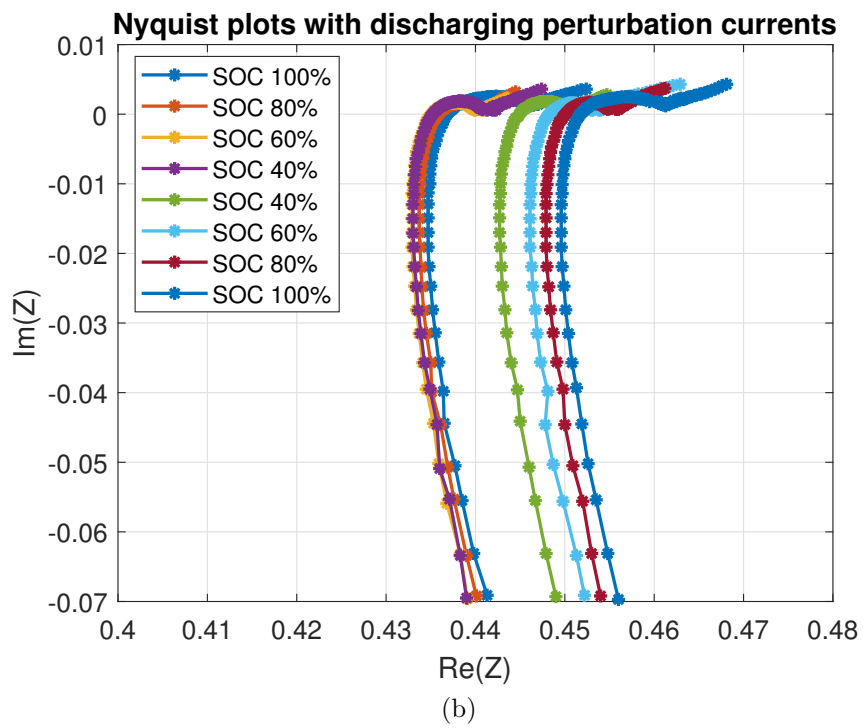
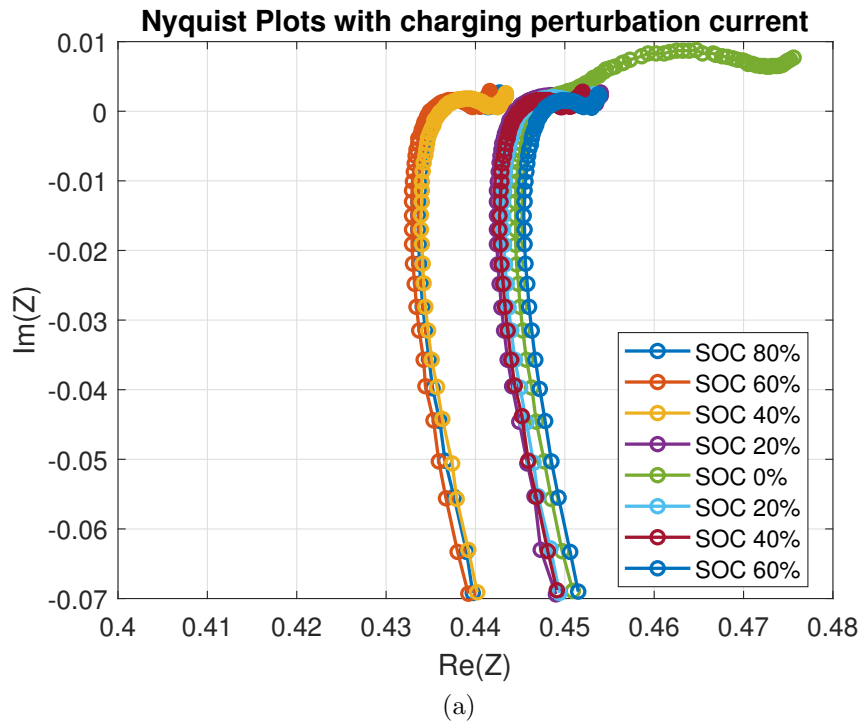


Figure 2.8: Nyquist plots for B3202

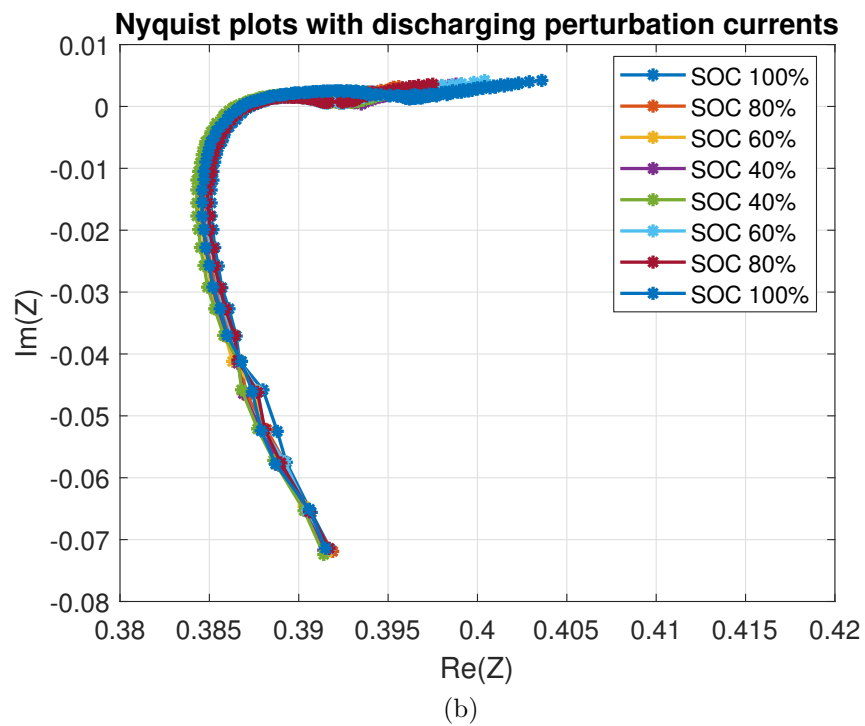
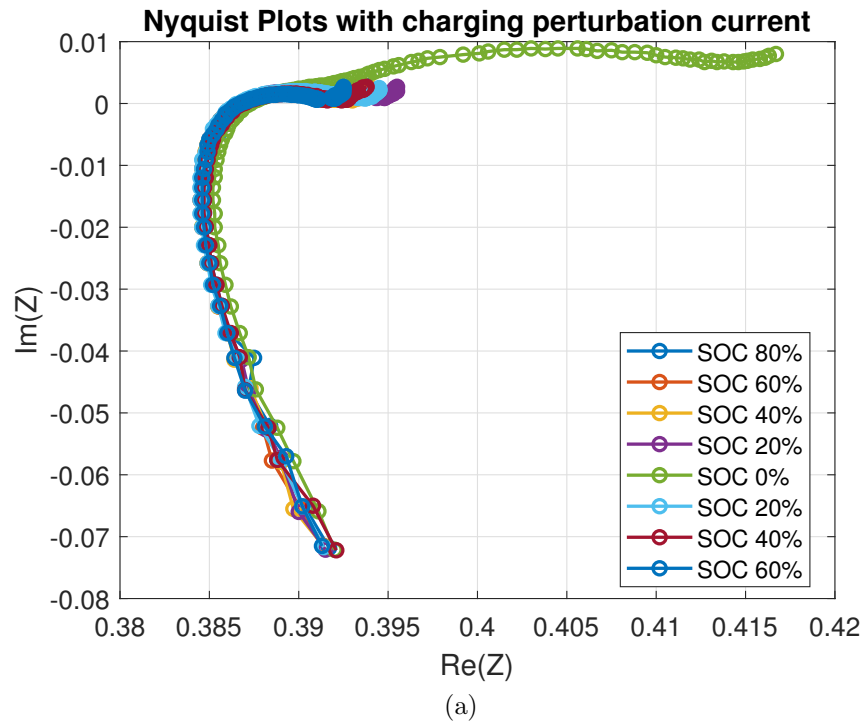


Figure 2.9: Nyquist plots for B3203

Battery	SOC	R_{Ω} $m\Omega$	R_{CT} $m\Omega$	R_{SEI} $m\Omega$	C_{DL} F	C_{SEI} F	L H	σ
B3201	100	345.45	4.9399	0	0.9831	0	1.0912e-06	0.004
	80	345.2667	3.2486	0	0.6832	0	1.0906e-06	0.0031
	60	345.1650	3.2316	0	0.6743	0	1.0900e-06	0.0024
	40	345.1850	3.4847	0	0.7084	0	1.0913e-06	0.0021
	20	345.1800	3.9727	0	0.7274	0	1.0920e-06	0.0005
	0	345.5600	4.2959	3.2	0.6718	0.9093	1.0932e-06	0.0057
B3202	100	446.26	5.0714	0	0.9147	0	1.117e-06	0.0044
	80	442.56	2.9568	0	0.6320	0	1.118e-06	0.0033
	60	443.40	3.1083	0	0.5980	0	1.118e-06	0.0026
	40	442.34	3.5562	0	0.6435	0	1.117e-06	0.0020
	20	447.06	3.8899	0	0.5983	0	1.1179e-06	0.0007
	0	448.72	5.5570	2.3	0.8026	0.61	1.1179e-06	0.0033
B3203	100	389.47	5.0045	0	0.9980	0	1.158e-06	0.0047
	80	389.36	3.3076	0	0.7612	0	1.159e-06	0.0032
	60	389.21	3.2182	0	0.7249	0	1.157e-06	0.0024
	40	389.145	3.5784	0	0.6841	0	1.159e-06	0.0022
	20	389.13	4.1240	0	0.7270	0	1.159e-06	0.0004
	0	389.84	4.9027	4.9	0.5797	0.7045	1.163e-06	0.0036

Figure 2.10: Estimated parameter values

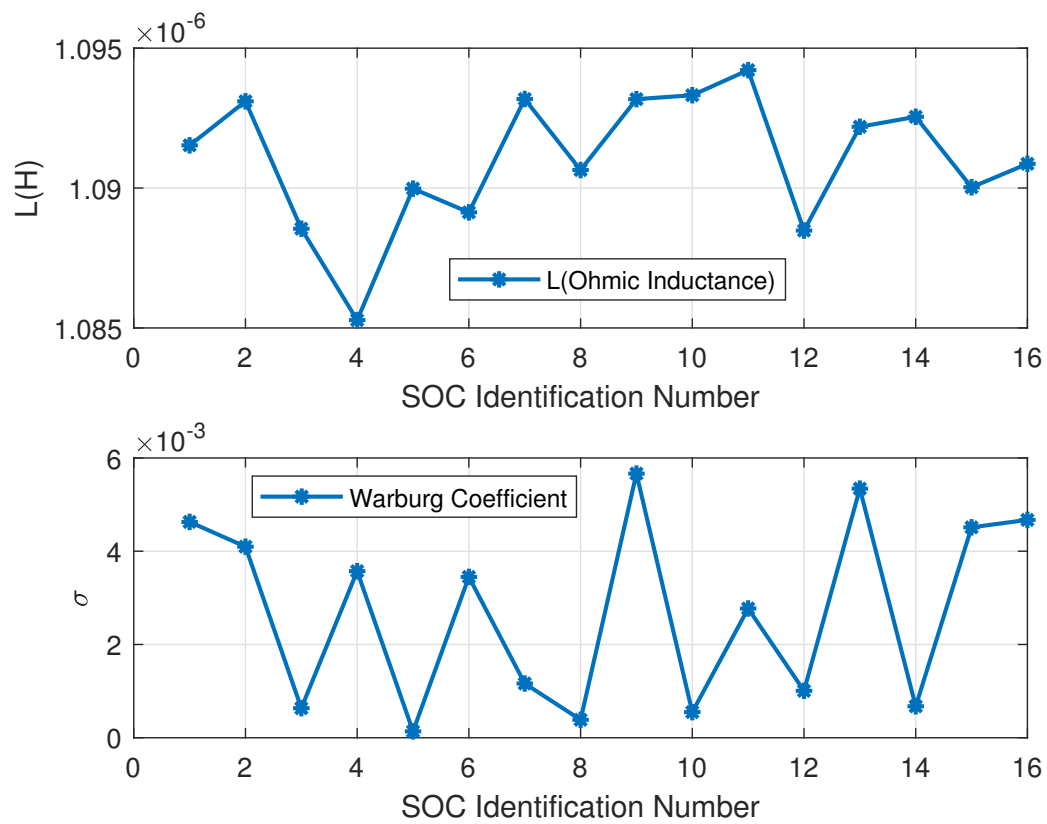


Figure 2.11: Estimated paramters for B3201 (Inductance and Warburg coefficient)

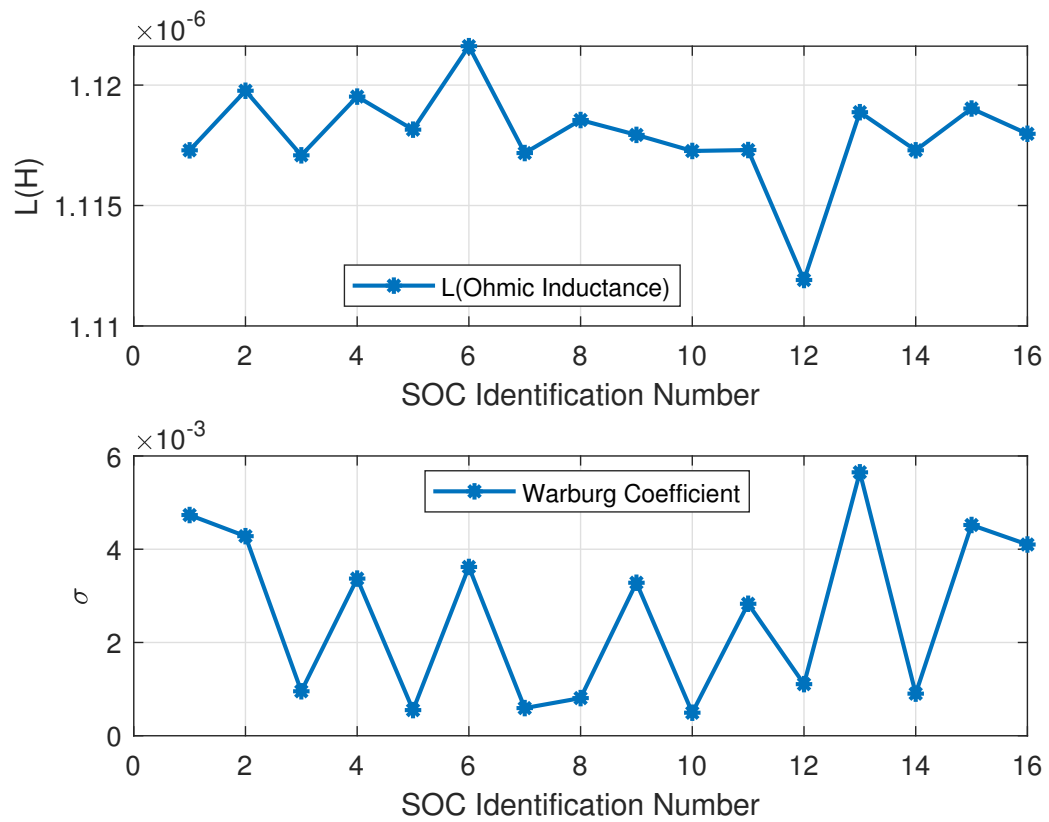


Figure 2.12: Estimated paramters for B3202 (Inductance and Warburg coefficient)

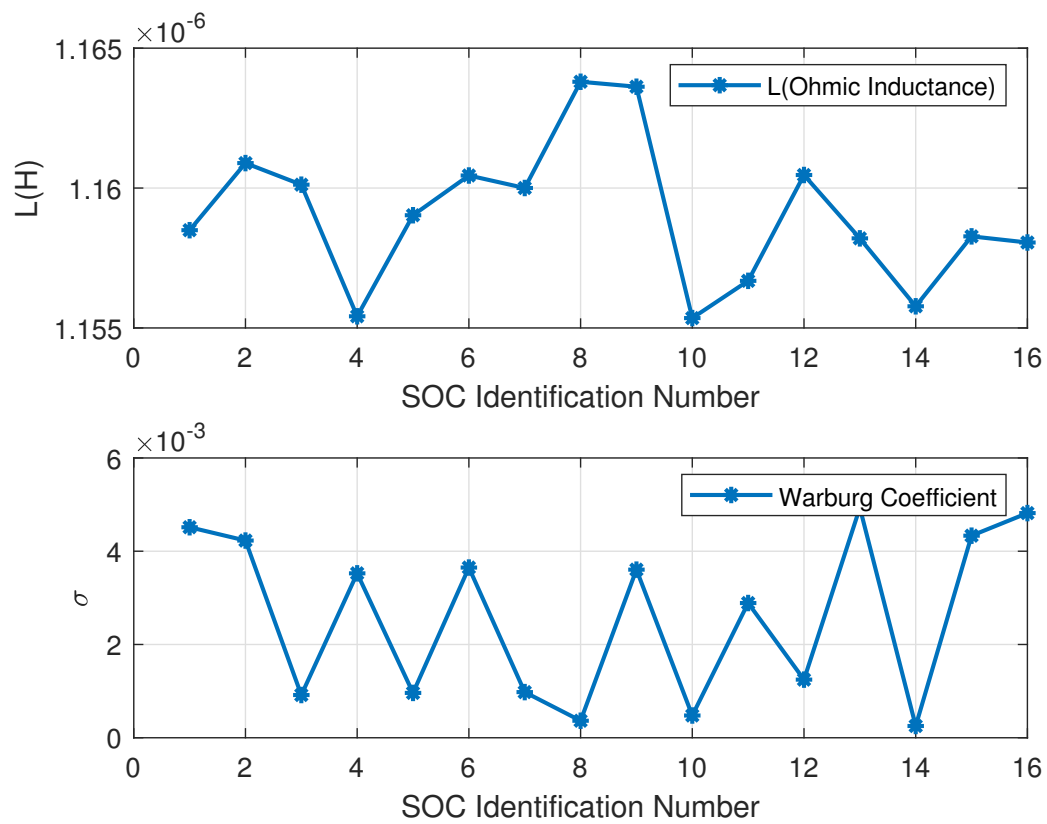


Figure 2.13: Estimated paramters for B3203 (Inductance and Warburg coefficient)

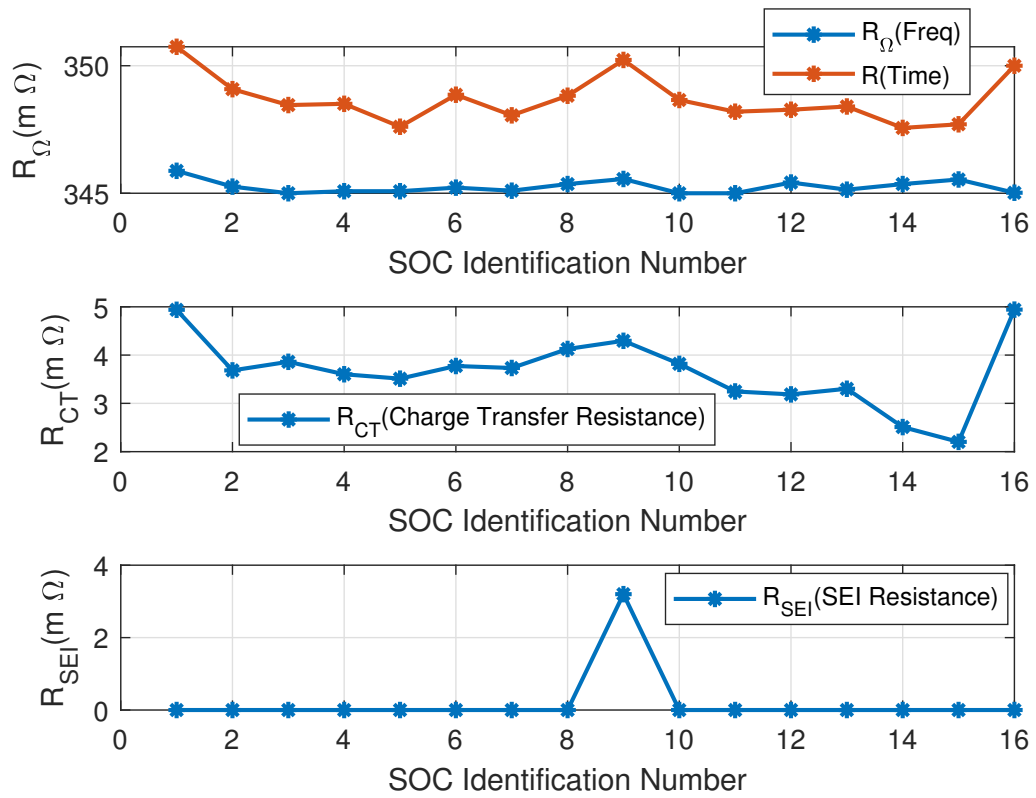


Figure 2.14: Estimated paramters for B3201 (Resistances)

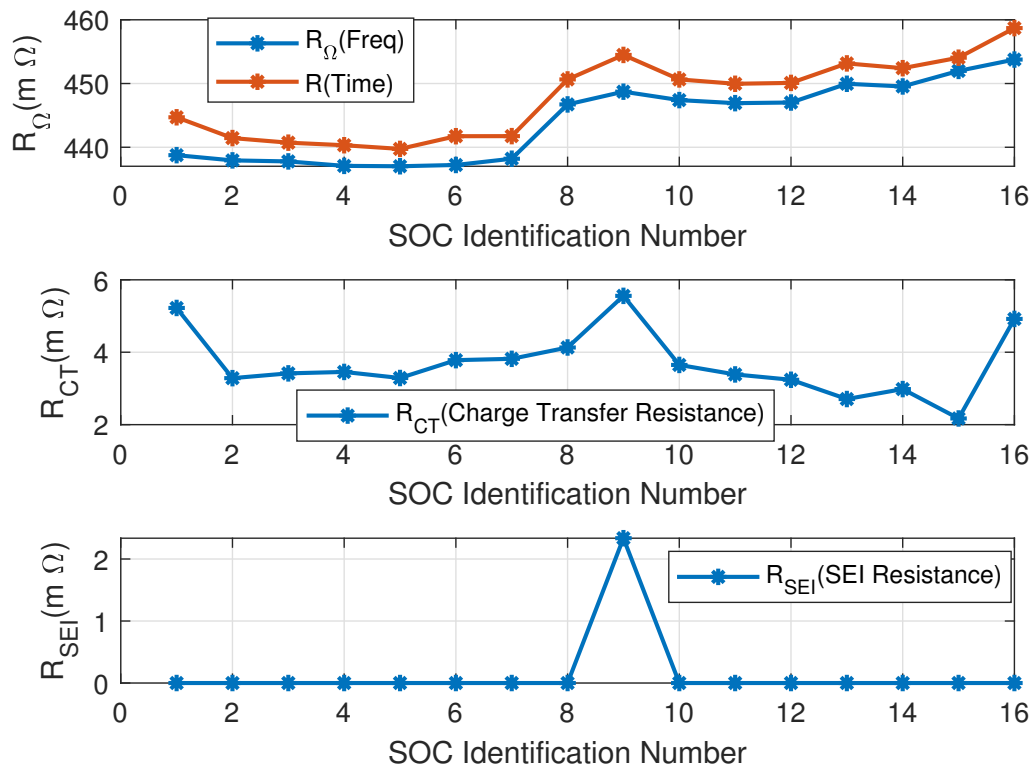


Figure 2.15: Estimated paramters for B3202 (Resistances)

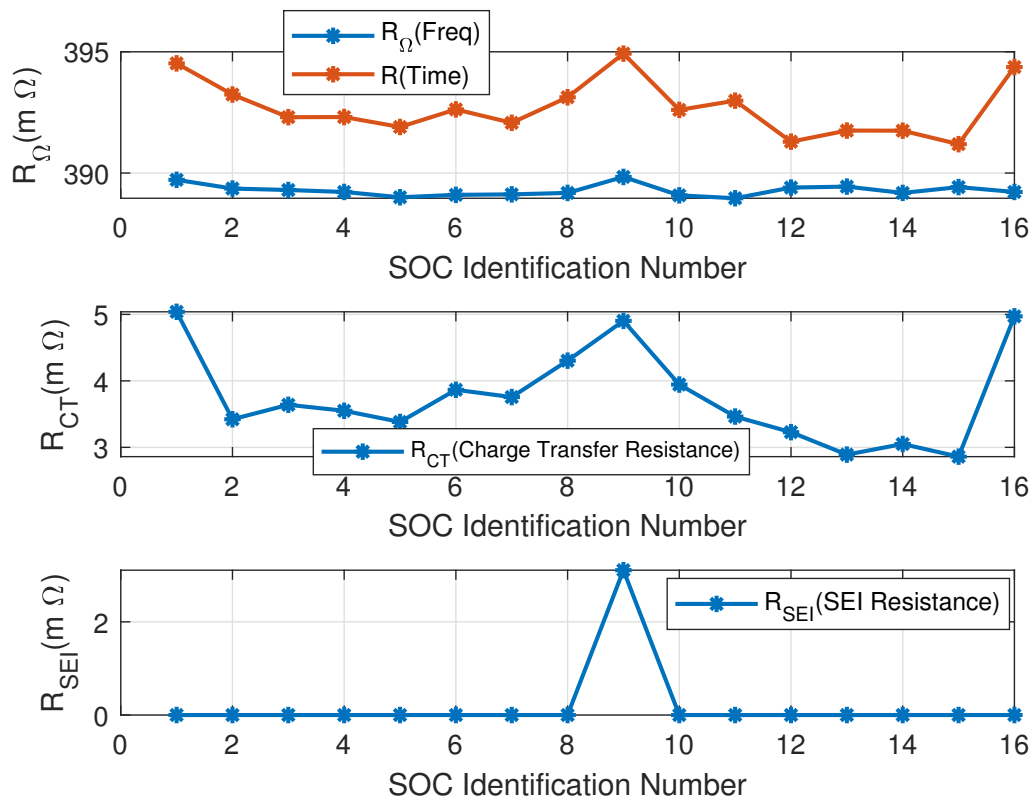


Figure 2.16: Estimated paramters for B3203 (Resistances)

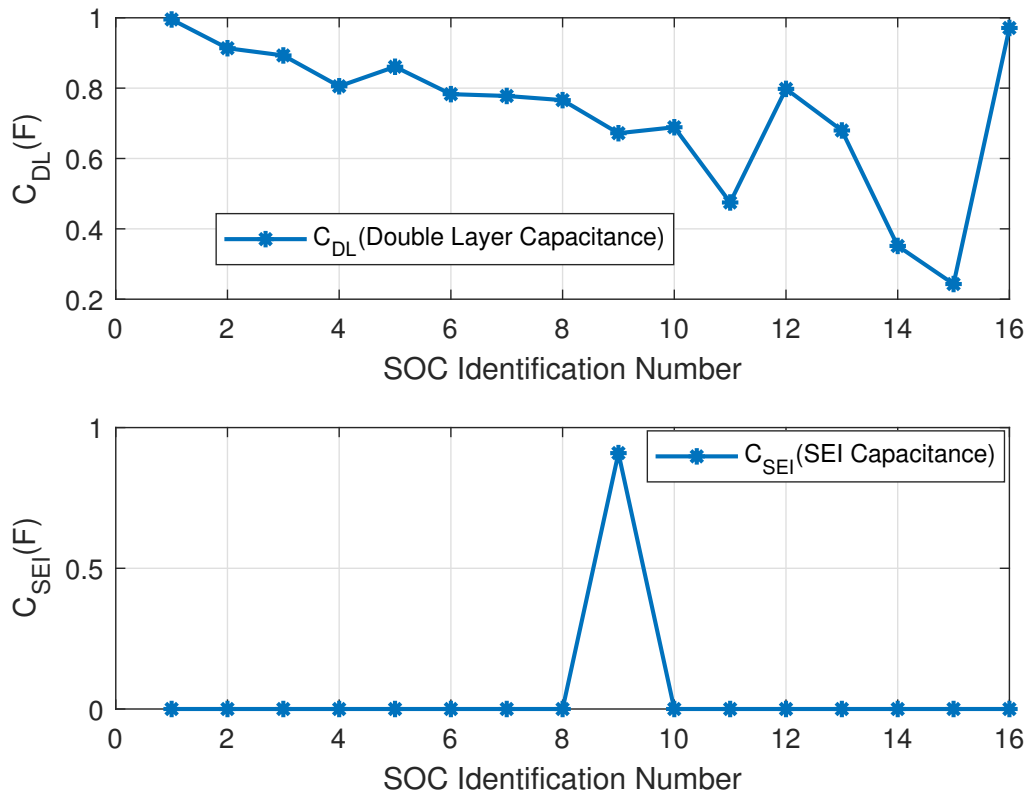


Figure 2.17: Estimated paramters for B3201 (Capacitances)

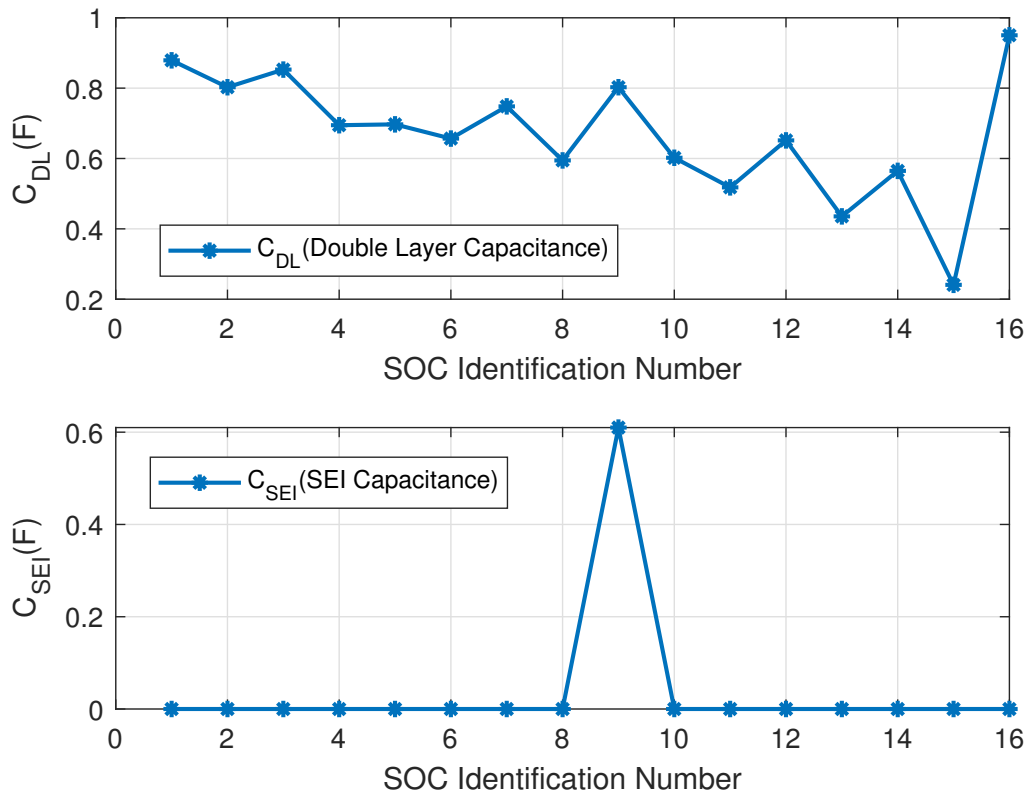


Figure 2.18: Estimated paramters for B3202 (Capacitances)

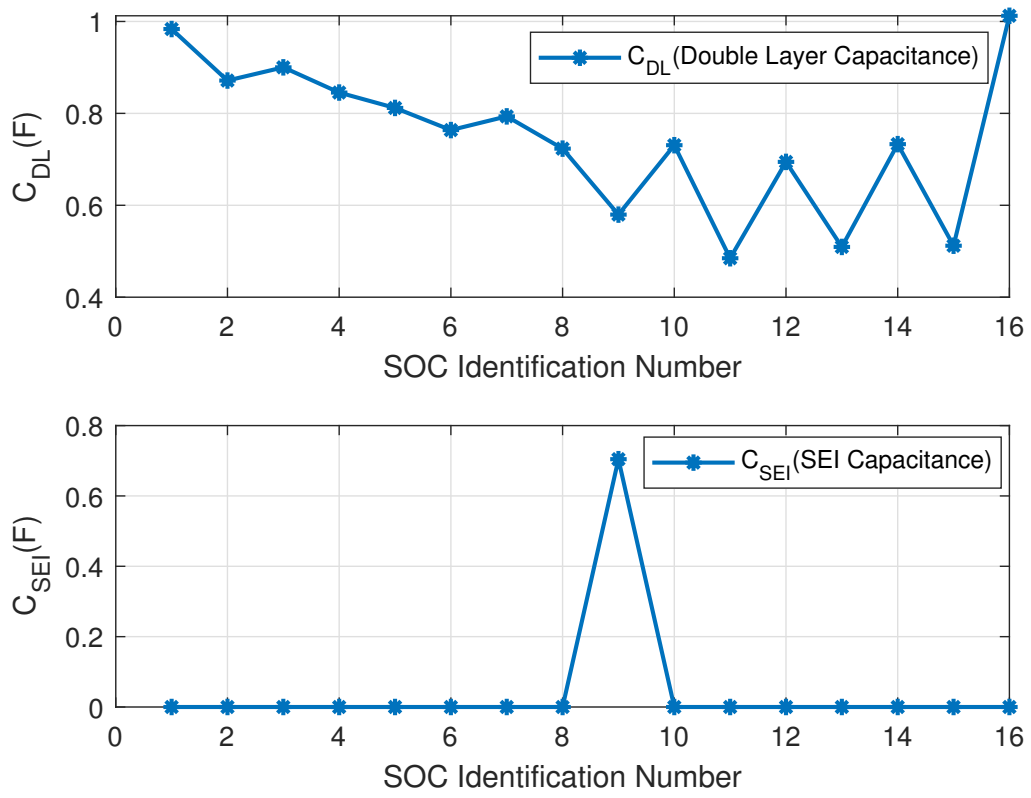


Figure 2.19: Estimated paramters for B3203 (Capacitances)

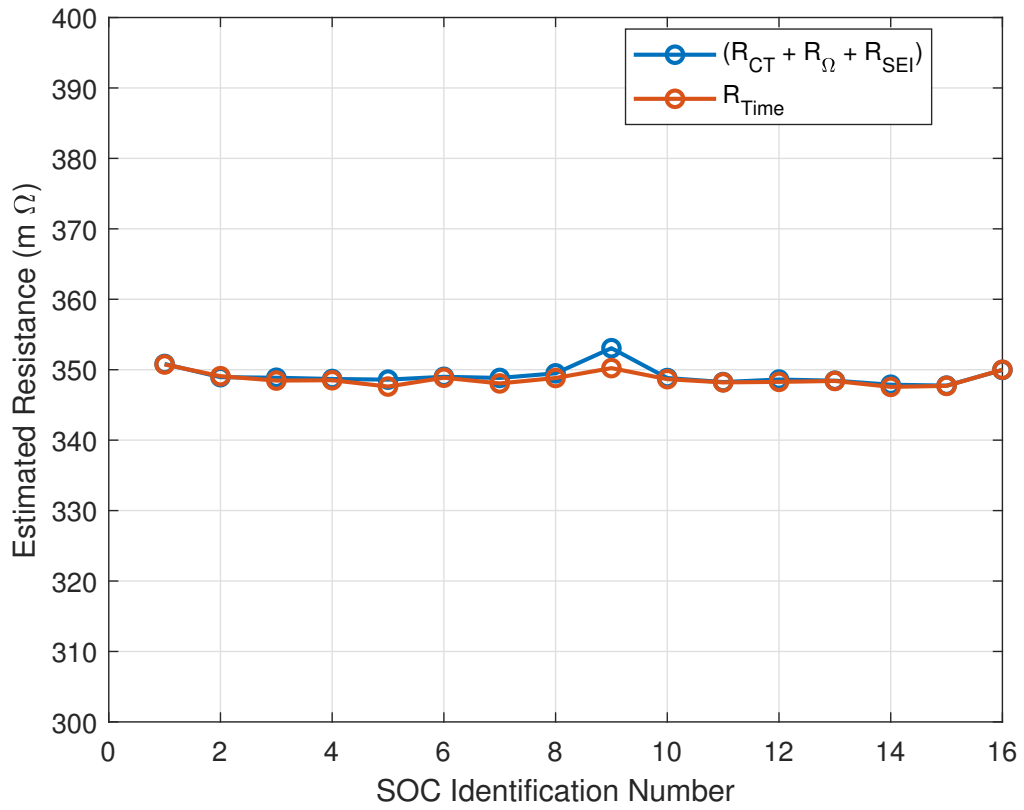


Figure 2.20: Estimated parameters for B3201 (Resistances in time domain and frequency domain)

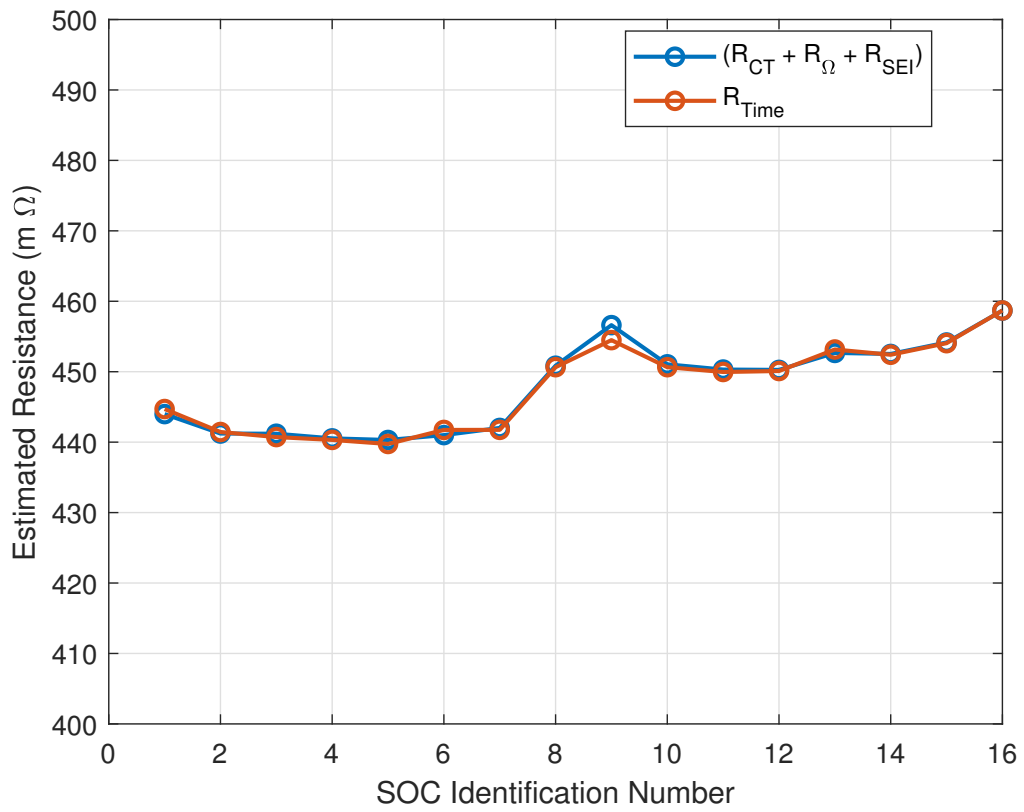


Figure 2.21: Estimated parameters for B3202 (Resistances in time domain and frequency domain)

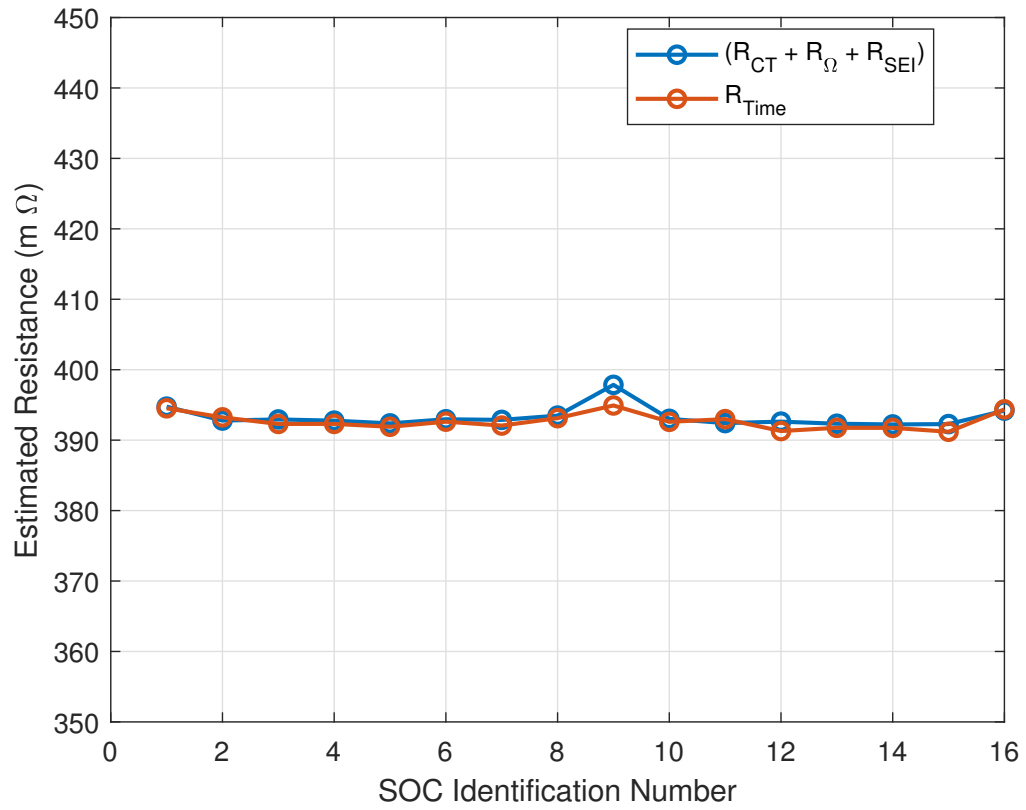


Figure 2.22: Estimated parameters for B3203 (Resistances in time domain and frequency domain)

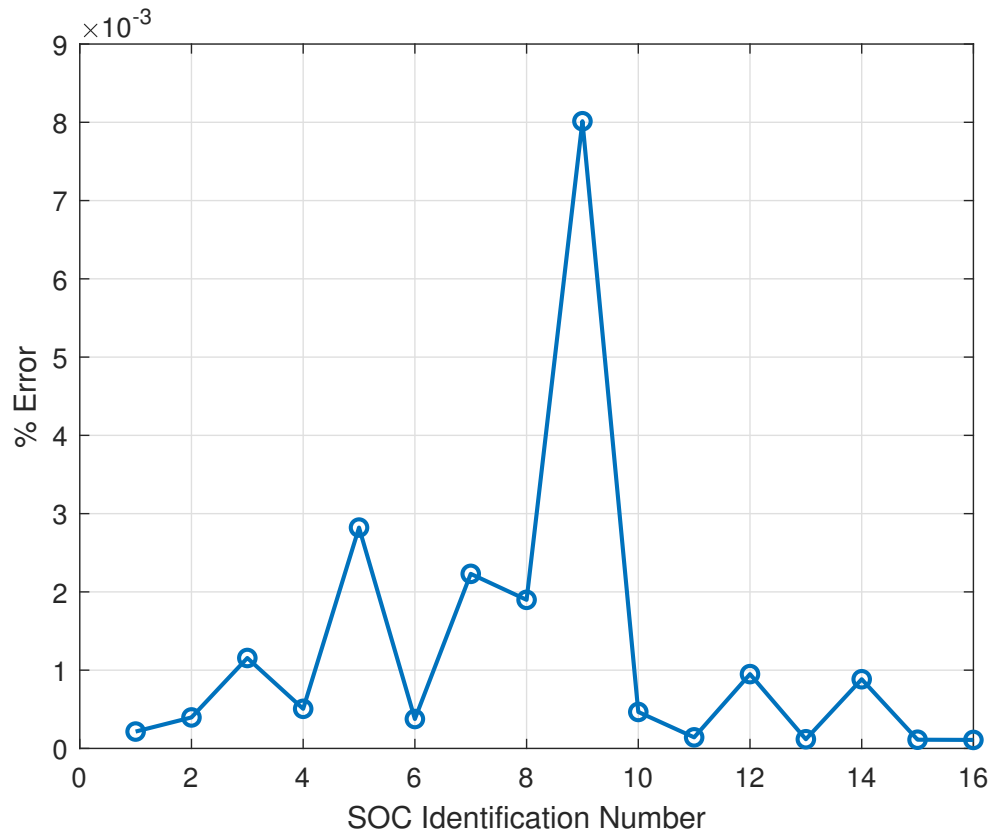


Figure 2.23: Percentage difference between time-domain and frequency domain estimates (B3201)

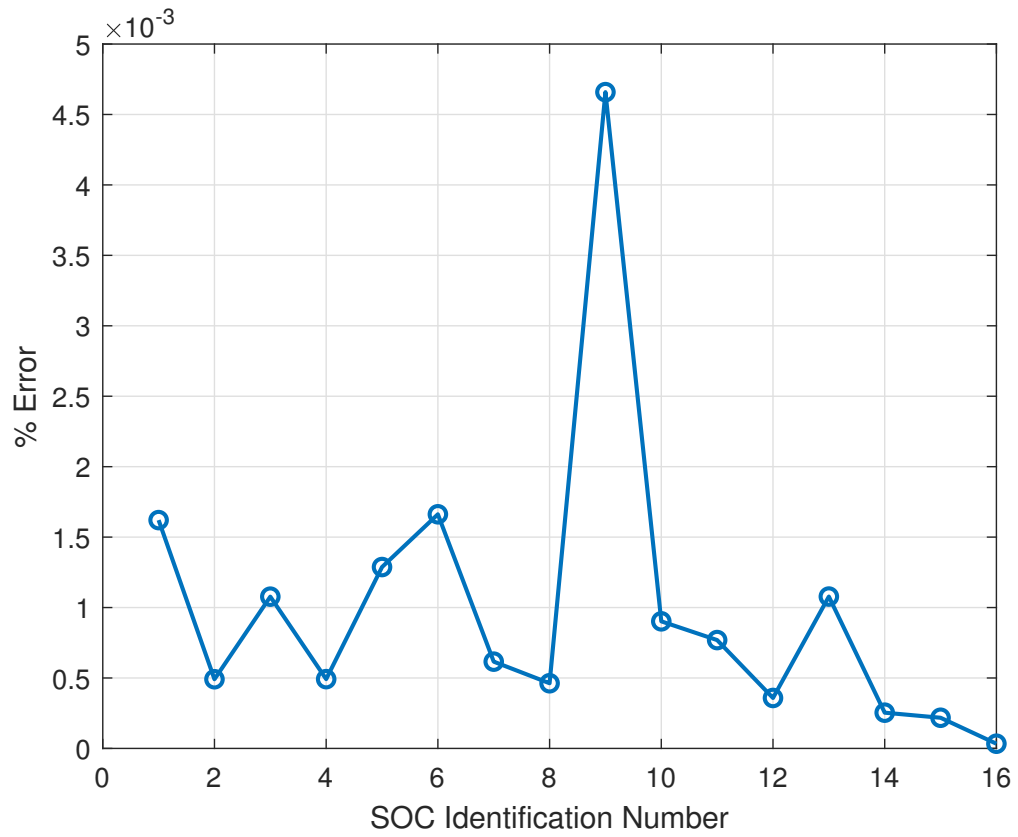


Figure 2.24: Percentage difference between time-domain and frequency domain estimates (B3202)

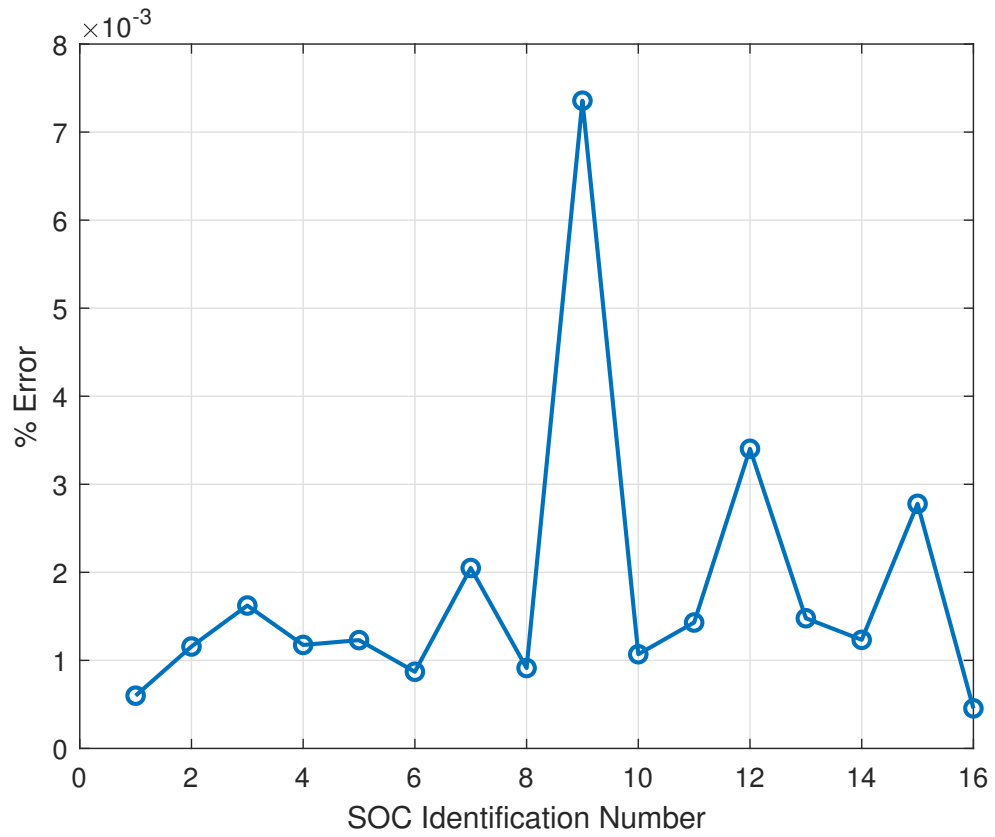


Figure 2.25: Percentage difference between time-domain and frequency domain estimates (B3203)

2.6 Conclusion

This paper presented an better approach to obtain battery ECM parameters using least square algorithms with multiple measurements. The algorithms are applied at real batteries at various SOC levels of the battery in both frequency and time domain. Battery impedance profile is obtained in the frequency domain along with current and voltage obtained in the time domain. The comparison of parameter estimated in frequency and time domain found to be very close with less than 0.01 percent error. In the paper, feature points ($k1, k2l, k2h, k3l, k3h$ and $k4$) are selected manually. Automatic selection of feature points can be done in future.

2.7 References

- [1] H. Movahedi, N. Tian, H. Fang, and R. Rajamani, “Hysteresis compensation and nonlinear observer design for state-of-charge estimation using a nonlinear double-capacitor li-ion battery model,” *IEEE/ASME Transactions on Mechatronics*, 2021. 5
- [2] B. Pattipati, B. Balasingam, G. Avvari, K. Pattipati, and Y. Bar-Shalom, “Open circuit voltage characterization of lithium-ion batteries,” *Journal of Power Sources*, vol. 269, pp. 317–333, 2014. 5
- [3] Y. Gao, X. Zhang, C. Zhu, and B. Guo, “Global parameter sensitivity analysis of electrochemical model for lithium-ion batteries considering aging,” *IEEE/ASME Transactions on Mechatronics*, vol. 26, no. 3, pp. 1283–1294, 2021. 5
- [4] Z. Deng, X. Hu, X. Lin, L. Xu, Y. Che, and L. Hu, “General discharge voltage information enabled health evaluation for lithium-ion batteries,” *IEEE/ASME Transactions on Mechatronics*, 2020. 5
- [5] M. S. Ahmed and B. Balasingam, “A scaling approach for improved open circuit voltage modeling in li-ion batteries,” in *2019 IEEE Electrical Power and Energy Conference (EPEC)*, pp. 1–6, IEEE, 2019. 5
- [6] B. Ospina Agudelo, W. Zamboni, and E. Monmasson, “A comparison of time-domain implementation methods for fractional-order battery impedance models,” *Energies*, vol. 14, no. 15, p. 4415, 2021. 6
- [7] B. Balasingam, G. Avvari, B. Pattipati, K. Pattipati, and Y. Bar-Shalom, “A robust approach to battery fuel gauging, part i: Real time model identification,” *Journal of Power Sources*, vol. 272, pp. 1142–1153, 2014. 6, 14

- [8] H. He, R. Xiong, and H. Guo, "Online estimation of model parameters and state-of-charge of lifepo4 batteries in electric vehicles," *Applied Energy*, vol. 89, no. 1, pp. 413–420, 2012. 6, 14
- [9] S. R. Islam and S.-Y. Park, "Precise online electrochemical impedance spectroscopy strategies for li-ion batteries," *IEEE Transactions on Industry Applications*, vol. 56, no. 2, pp. 1661–1669, 2019. 6
- [10] O. Heaviside, "Electrical papers by oliver heaviside (in two volumes)," *New York: MacMillon & Co*, vol. 268, 1894. 6
- [11] M. E. Orazem and B. Tribollet, "Electrochemical impedance spectroscopy," *New Jersey*, pp. 383–389, 2008. 6
- [12] M. D. Murbach and D. T. Schwartz, "Analysis of li-ion battery electrochemical impedance spectroscopy data: An easy-to-implement approach for physics-based parameter estimation using an open-source tool," *Journal of The Electrochemical Society*, vol. 165, no. 2, p. A297, 2018. 6
- [13] B. Pattipati, C. Sankavaram, and K. Pattipati, "System identification and estimation framework for pivotal automotive battery management system characteristics," *IEEE Transactions on Systems, Man, and Cybernetics, Part C (Applications and Reviews)*, vol. 41, no. 6, pp. 869–884, 2011. 6
- [14] J. Xu, C. C. Mi, B. Cao, and J. Cao, "A new method to estimate the state of charge of lithium-ion batteries based on the battery impedance model," *Journal of power sources*, vol. 233, pp. 277–284, 2013. 6
- [15] Q. Yang, J. Xu, B. Cao, and X. Li, "A simplified fractional order impedance model and parameter identification method for lithium-ion batteries," *PLoS One*, vol. 12, no. 2, p. e0172424, 2017. 6, 7

- [16] C. Pastor-Fernández, W. D. Widanage, J. Marco, M.-Á. Gama-Valdez, and G. H. Chouchelamane, “Identification and quantification of ageing mechanisms in lithium-ion batteries using the eis technique,” in *2016 IEEE Transportation Electrification Conference and Expo (ITEC)*, pp. 1–6, IEEE, 2016. 6
- [17] J. A. A. Qahouq and Z. Xia, “Single-perturbation-cycle online battery impedance spectrum measurement method with closed-loop control of power converter,” *IEEE Transactions on Industrial Electronics*, vol. 64, no. 9, pp. 7019–7029, 2017. 6
- [18] B. Agudelo, W. Zamboni, E. Monmasson, and G. Spagnuolo, “Identification of battery circuit model from eis data,” in *JCGE-Congrès des Jeunes Chercheurs en Génie Electrique*, 2019. 6
- [19] S. Islam, S.-Y. Park, and B. Balasingam, “Unification of internal resistance estimation methods for li-ion batteries using hysteresis-free equivalent circuit models,” *Batteries*, vol. 6, no. 2, p. 32, 2020. 6
- [20] A. Kersten, M. Kuder, W. Han, T. Thiringer, A. Lesnicar, T. Weyh, and R. Ecklerle, “Online and on-board battery impedance estimation of battery cells, modules or packs in a reconfigurable battery system or multilevel inverter,” in *IECON 2020 The 46th Annual Conference of the IEEE Industrial Electronics Society*, pp. 1884–1891, IEEE, 2020. 6, 7
- [21] M. Galeotti, L. Cinà, C. Giammanco, S. Cordiner, and A. Di Carlo, “Performance analysis and soh (state of health) evaluation of lithium polymer batteries through electrochemical impedance spectroscopy,” *Energy*, vol. 89, pp. 678–686, 2015. 7
- [22] J. Jiang, W. Shi, J. Zheng, P. Zuo, J. Xiao, X. Chen, W. Xu, and J.-G. Zhang, “Optimized operating range for large-format lifepo4/graphite batteries,” *Journal of The Electrochemical Society*, vol. 161, no. 3, p. A336, 2013. 7

- [23] B. Balasingam and K. R. Pattipati, “On the identification of electrical equivalent circuit models based on noisy measurements,” *IEEE Transactions on Instrumentation and Measurement*, vol. 70, pp. 1–16, 2021. 8, 14
- [24] W. Waag, S. Käbitz, and D. U. Sauer, “Experimental investigation of the lithium-ion battery impedance characteristic at various conditions and aging states and its influence on the application,” *Applied energy*, vol. 102, pp. 885–897, 2013. 8
- [25] M. A. Ghadi, *Performance Analysis and Improvement of Electrochemical Impedance Spectroscopy for Online Estimation of Battery Parameters*. PhD thesis, University of Windsor (Canada), 2021. 9, 10

Chapter 3

Electrochemical Impedance

Spectroscopy with Reduced Time

Signal

3.1 Introduction

The electrochemical energy storage has emerged as a key technology that can play a key role in the improvement of energy sustainability in most of the areas in daily lives [1]. The widespread adoption of renewable energy and distributed generation in power networks, as well as the growing use of electric mobility, have all become key fields of interest for energy storage systems [2].

Li-Ion batteries have become the most important energy storage for Electric and Hybrid Vehicles (EV and HEV) applications due to their high power and energy density, high efficiency, extended cycle life, and minimal self-discharge. Nonetheless, Li-Ion batteries are expensive and more susceptible to operating conditions such as useable capacity [3], temperature [4], power consumption, and lifetime owing to ageing [5]. As a result, in the automotive field, continual evaluation and forecast of battery performance and service life (battery states) are important criteria for consumers. The

electronic control unit known as the Battery Management System (BMS) is commonly used in Li-Ion batteries to monitor battery state and execute reliable operations.

Electrochemical impedance spectroscopy (EIS) is a powerful technique used in domains as diverse as energy, electrocatalysis, materials science [6–9] and medication. EIS is very good technique to obtain physical properties such as diffusion coefficient and chemical reaction rates and microstructural characteristics of the electrochemical (EC) system under study [10, 11]. Among all the traditional EC approaches, EIS stands apart because it assesses the relationship between the current and the potential difference in the frequency domain [10]. EIS has gained its importance among the characterization of batteries [12]. There are many advantages to using electrochemical impedance spectroscopy (EIS) for understanding the power delivery capability in lithium-ion battery systems. EIS can separate and quantify the cell resistance of the bulk (R_b), interface layer (R_{SEI}), charge transfer reaction (R_{ct}), and diffusion process (W) by a single experiment [13]. While EIS is an appealing technique that has been widely utilised to evaluate performance characteristics, [14–16] there are issues with the lengthy processing time necessary, as well as the size and weight of the equipment required to do the study. As a result of these problems, [17, 18] EIS is not frequently used as an on-line tool for non-invasive diagnosis and concurrent control.

In this paper an approach to perform EIS with less time is proposed. The approach involves construction of a perturbation current signal in such a way that wide range of frequencies can be swept in a sine wave signal. Unlike chirp signal, the conversion to frequency domain can be done using fast Fourier transform with less spectral leakage. Therefore, the approach outperforms the existing EIS techniques in providing impedance response of the battery in less time.

The remainder of the paper is organized as follows, Section II describes the construction of fast perturbation current signal with varying frequencies. Section III demonstrates the process of obtaining the impedance spectrum of battery using the signal explained in section II. Results are shown in section IV. Section V concludes

the paper.

3.2 Construction of Perturbation Current Signal

The signal consists of a combination of multiple sinewaves with different frequencies. Each sinewave is divided into an equal number of segments. Every segments corresponds to a particular frequency. The frequency ranges from 0.01 Hz to 10kHz which is fragmented linearly so as to obtain a smooth signal. After fragmentation of frequencies it was found that from 0.01 Hz to 10kHz it got divided into 829 parts. The process of signal construction is explained.

Some notations used in the calculations are:

$n = 2$ times number of frequency segments in a sine wave

$s =$ number of sampled parts in each segment

$f =$ frequency for which sinewave segment is constructed

$\phi =$ angle swept by the signal

$t_s =$ sampling time

$t_c =$ time to cover constant phase angle at particular frequency

$t_p =$ time to cover previous angle of the signal at current frequency

$t_f =$ time for generating sine wave

$t_\alpha =$ actual time vector

$S =$ signal amplitude

$i = 1, 2, \dots, 829$

Angle swept by each segment of sine wave can be written as

$$\phi_i = i \frac{\pi}{n} \quad (3.28)$$

Time to cover constant angle of $\frac{\pi}{n}$ at particular frequency can be written as

$$t_{c_i} = \frac{1}{2f_i n} \quad (3.29)$$

The sampling time for each frequency can be written as

$$t_{s_i} = \frac{t_{c_i}}{s} \quad (3.30)$$

where s is number of sampled fragments.

Time taken to cover previous angle by the current frequency sine wave

$$t_{p_i} = \frac{\phi_{i-1}}{2\pi f_i} \quad (3.31)$$

Time vectors for generating sine wave at different frequency can be written as

$$t_{f_i} = t_{p_i} \underbrace{[1 \ 1 \ \dots \ 1]}_s + \underbrace{[0 \ it_{s_i} \ \dots \ t_{c_i} - t_{s_i}]}_s \quad (3.32)$$

and

$$T_f = \underbrace{[t_{f_1} \ t_{f_2} \ \dots \ t_{f_i}]}_{829} \quad (3.33)$$

$$(3.34)$$

Actual time vector for the signal

$$t_{\alpha_i} = t_{c_i} \underbrace{[1 \ 1 \ \dots \ 1]}_s + \underbrace{[0 \ it_{s_i} \ \dots \ t_{c_i} - t_{s_i}]}_s \quad (3.35)$$

and (3.36)

$$T_{\alpha} = \underbrace{[t_{\alpha_1} \ t_{\alpha_2} \ \dots \ t_{\alpha_i}]}_{829} \quad (3.37)$$

(3.38)

Hence, signal amplitude can be written as

$$S_{\alpha_i} = \sin(2\pi f_i t_{f_i}) \quad (3.39)$$

and

$$S_{\alpha} = [S_{\alpha_1} \ S_{\alpha_2} \ \dots \ S_{\alpha_i}] \quad (3.40)$$

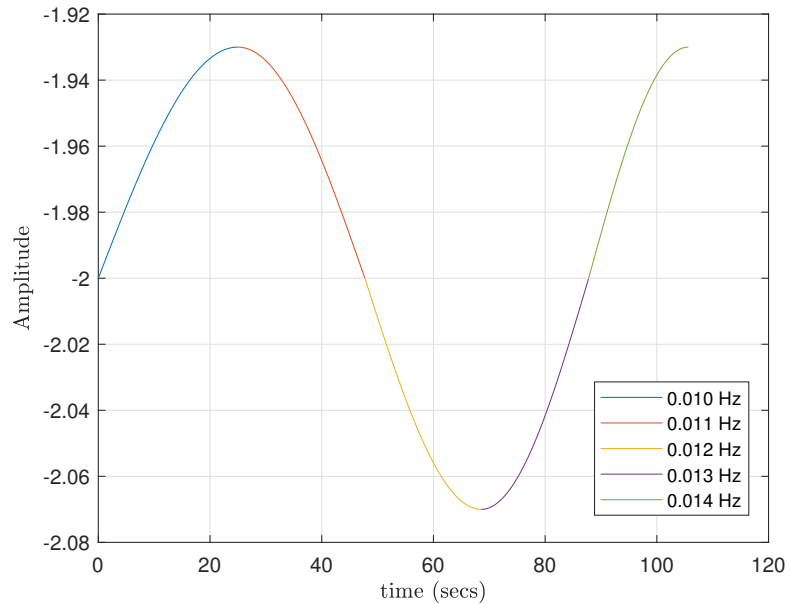


Figure 3.26: **Sine wave with n = 2**

(Since n = 2 each sine wave is constructed using 5 frequencies)

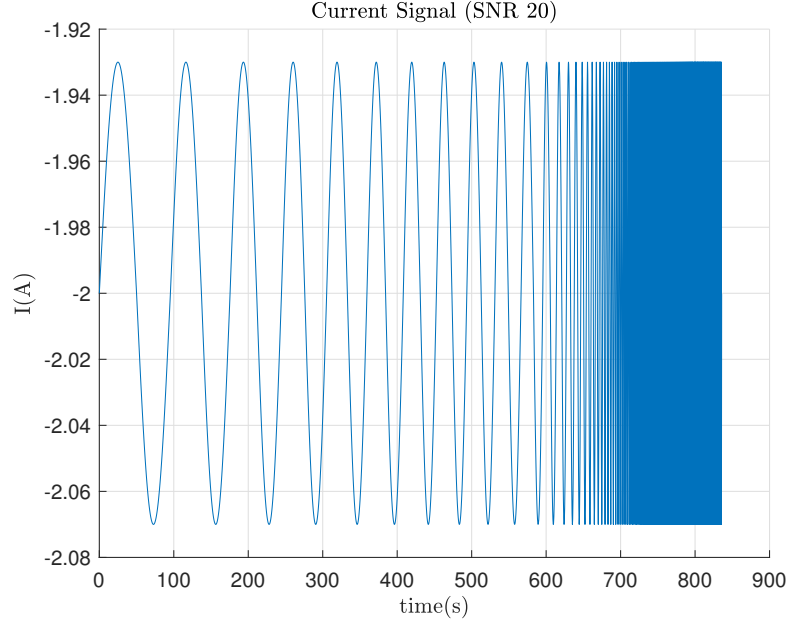


Figure 3.27: **Sine wave with $n = 2$**

Figure 3.26 shows the signal constructed using Equations 3.28 - 3.40 for 5 frequencies when $n = 2$. Figure 3.27 shows the full perturbation signal for $n = 2$.

3.3 Obtaining the Nyquist Plots

Once the current signal is constructed, it is applied to the battery and its voltage response is recorded. These time domain current signal and voltage response of the battery are converted to frequency domain using fast Fourier transform technique (FFT). Let us assume I_F as current signal and V_F as the measured voltage converted to the frequency domain using FFT.

Impedance (Z_F) of the battery can be written as

$$Z_F = \frac{V_F}{I_F} \quad (3.41)$$

The real part of the obtained impedance is plotted against the negative imaginary

part of the impedance. This impedance plot is known as Nyquist plot. The parameters are obtained from the Nyquist plot according to the adaptive Randles equivalent circuit model [12] using least square estimation techniques.

3.4 Results

In order to obtain the impedance spectrum, simulation is done for a 1000mAh Li-ion battery whose parameters are taken from [12]. Perturbation signal is constructed using $n = 2, 4$ and 6 . The perturbation current signal at different values of n is shown in Figure 3.28. The corresponding Nyquist plots with varying SNR are shown in Figure 3.29, 3.30 and 3.31. From Figures 3.28 to 3.31, it can be clearly seen that as n increases the Nyquist plot at lower SNR (SNR 40) becomes noisy. This is caused by spectral leakage caused during conversion into frequency domain through the fast Fourier transform. As the signal length decreases, the spectral leakage increases which causes noise in the Nyquist plot at lower SNR. Parameters of the battery are estimated using the Nyquist plots from SNR 40 to SNR 80. Errors in the parameters with respect to different SNRs are shown in Figure 3.32, 3.33, 3.34, 3.35, 3.36 and 3.38. All the parameters are estimated at different values of n . Figure 3.32, shows the estimated ohmic resistance. Estimates of ohmic resistances at different SNR found to be under 0.06 % error. Figure 3.33 depicts the estimated stray inductance which was found to be under 10% error at lower SNR and under 5% at higher SNR. Estimated charge transfer resistance (R_{CT}) and double layer capacitance (C_{DL}) are shown in Figure 3.35 and Figure 3.36. In the Figures, 3.35 and Figure 3.36 errors at lower SNR is comparatively higher than errors in ohmic resistance, stray inductance. This is because of the non-linear nature of CT arc which makes the curve fitting more sensitive to noise. Eventually, estimated Warburg impedance (σ), resistance due to Solid electrolyte interface (SEI) layer and capacitance due to SEI layer with respect to different SNRs are shown in Figures 3.34, 3.37 and 3.38. At lower SNRs C_{SEI} found

to be showing very high errors which limits the algorithms to work only at higher SNRs. This is because C_{SEI} is estimated from curve fitting of SEI arc which has i) less number of points, ii) more noise as n increases.

Parameters are estimated at different SNRs and different values of n .

3.5 Conclusion

This paper presents a novel approach for performing Electrochemical impedance spectroscopy with reduced time and its effect on impedance response of the battery. Even though EIS is well known technique, its application is limited either in laboratories for high precision instruments or in industries for impedance testing at high frequency which takes less time. EIS at frequencies ranging from very low (0.01 Hz) to very high (10kHz) consumes a lot of time with the traditional method. The average time taken by an EIS machine in this frequency range is approximately one hour. A new approach is developed to perform an EIS in reduced time. However, as time taken in EIS is reduced, it increases noise in the Nyquist plots. Parameters are obtained from the Nyquist plots. Error analysis of the parameters shows that at the EIS time reduces, higher SNR is required for the parameters of the battery to be estimated correctly. .

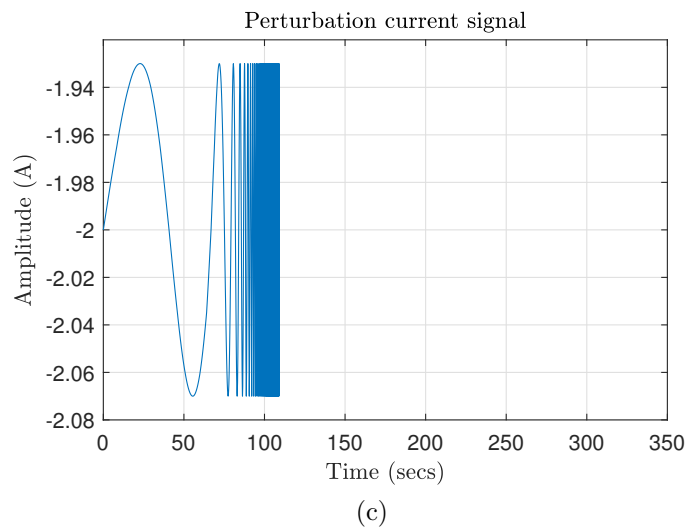
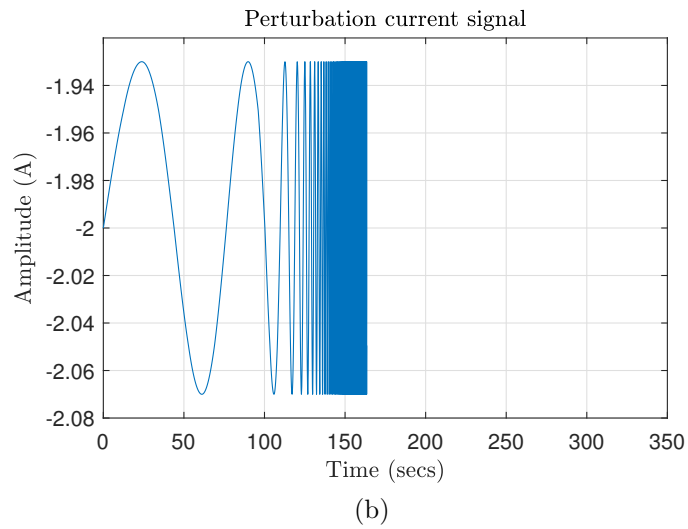
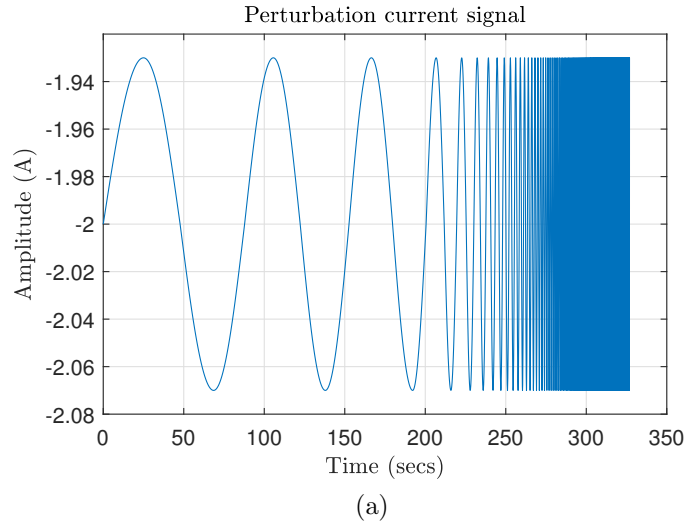


Figure 3.28: **Current signal for (a) $n = 2$, (b) $n = 4$, (c) $n = 6$**

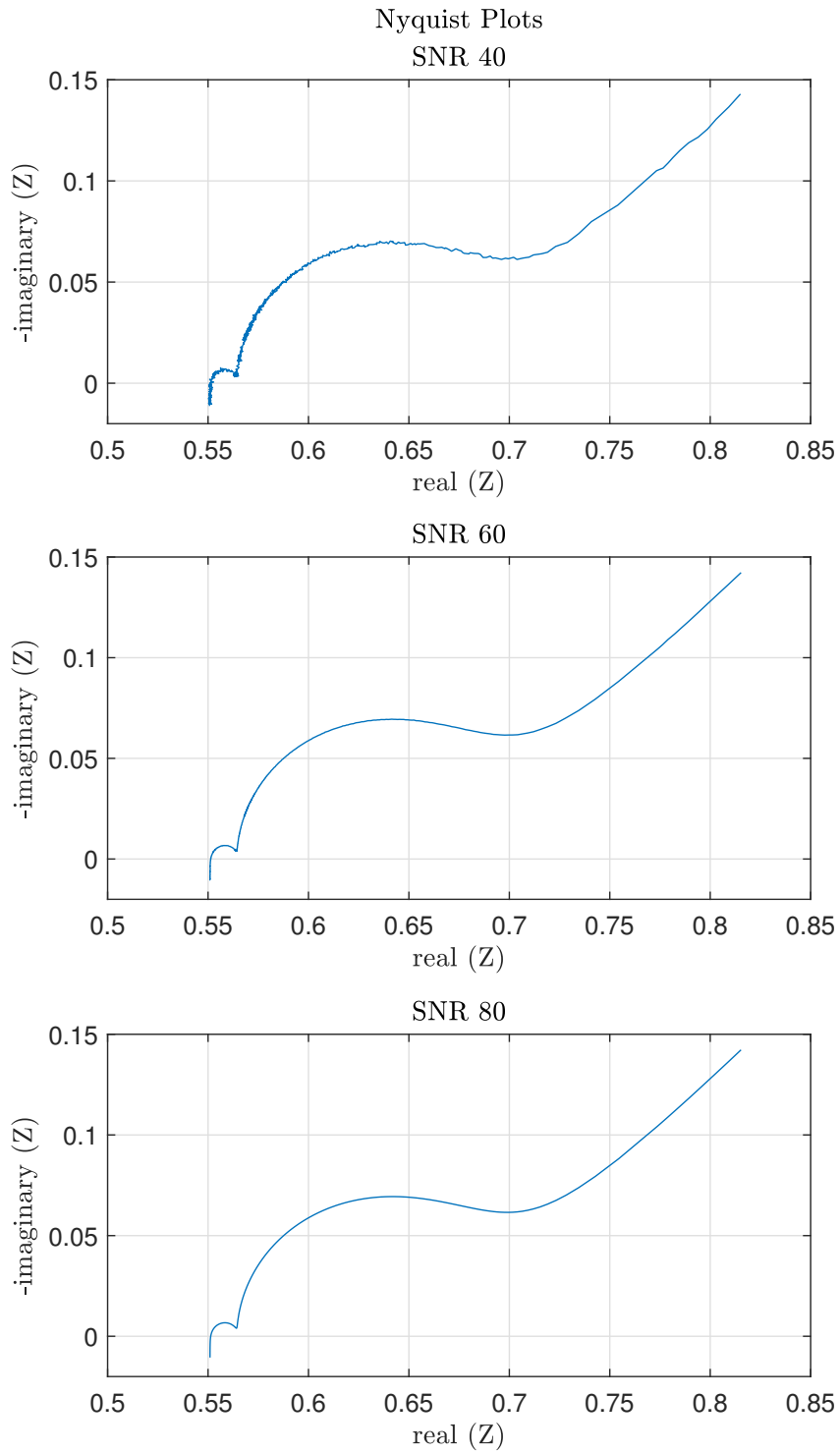


Figure 3.29: Nyquist plots for $n = 2$

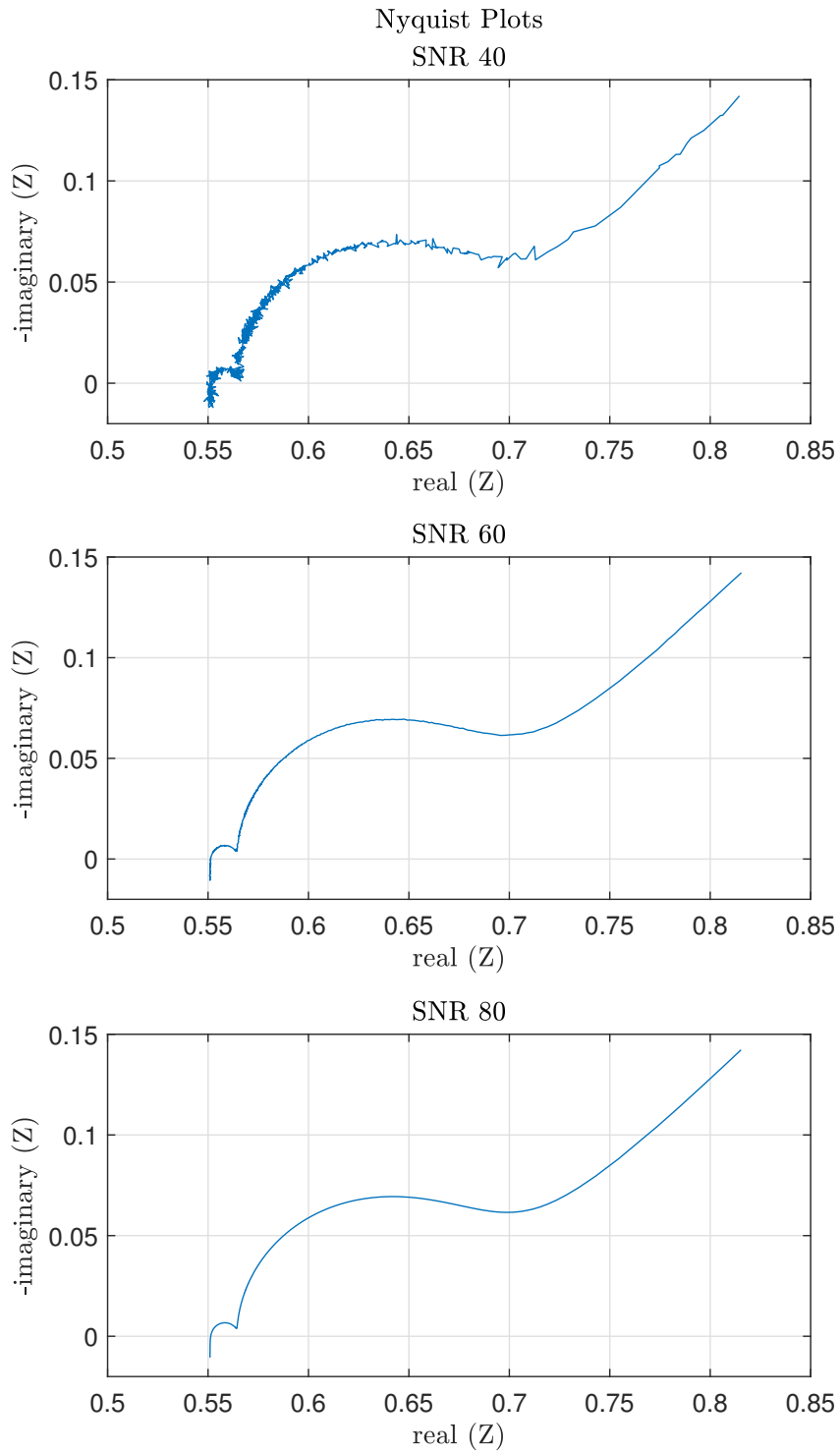


Figure 3.30: Nyquist plots for $n = 4$

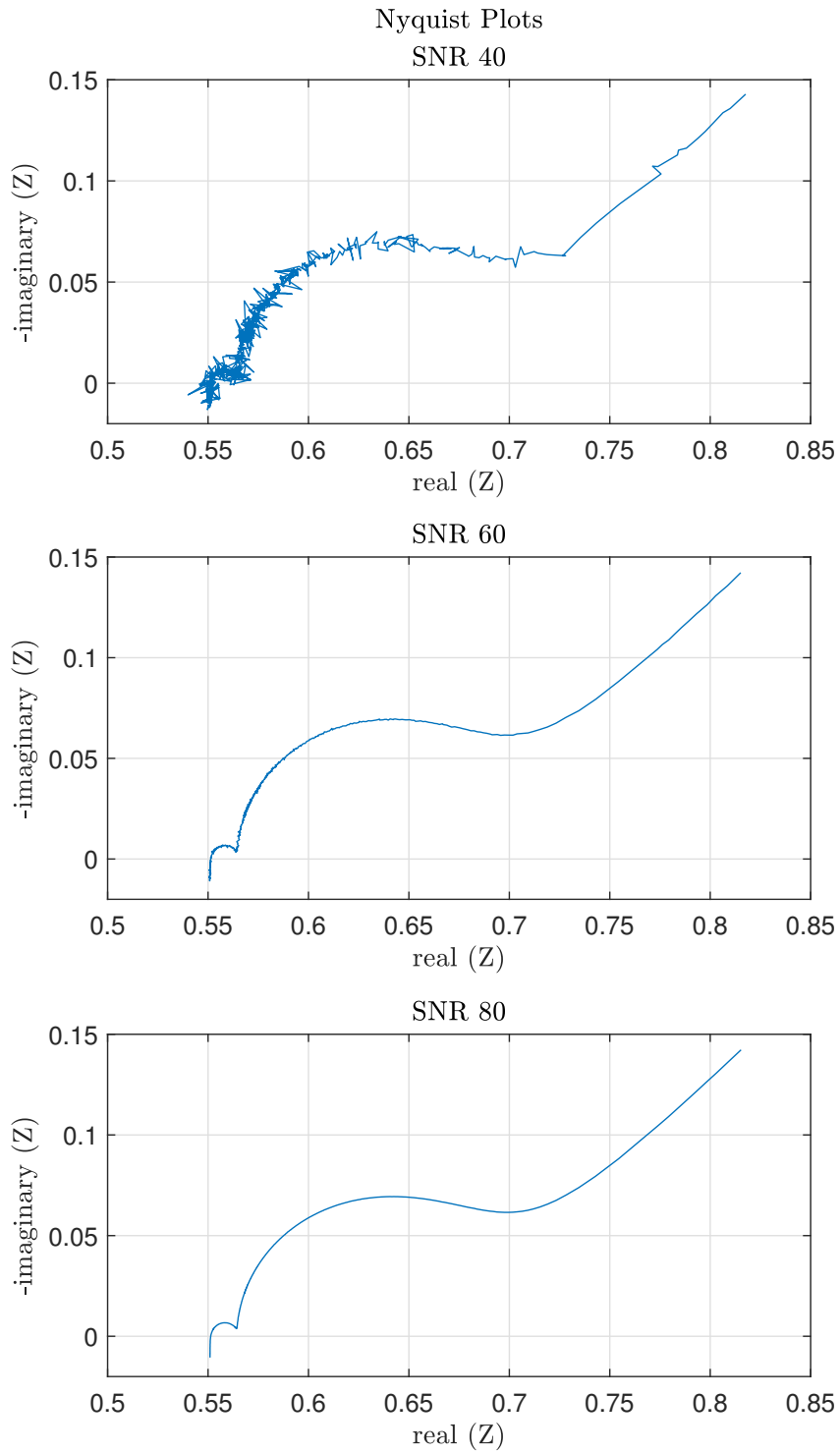


Figure 3.31: Nyquist plots for $n = 6$

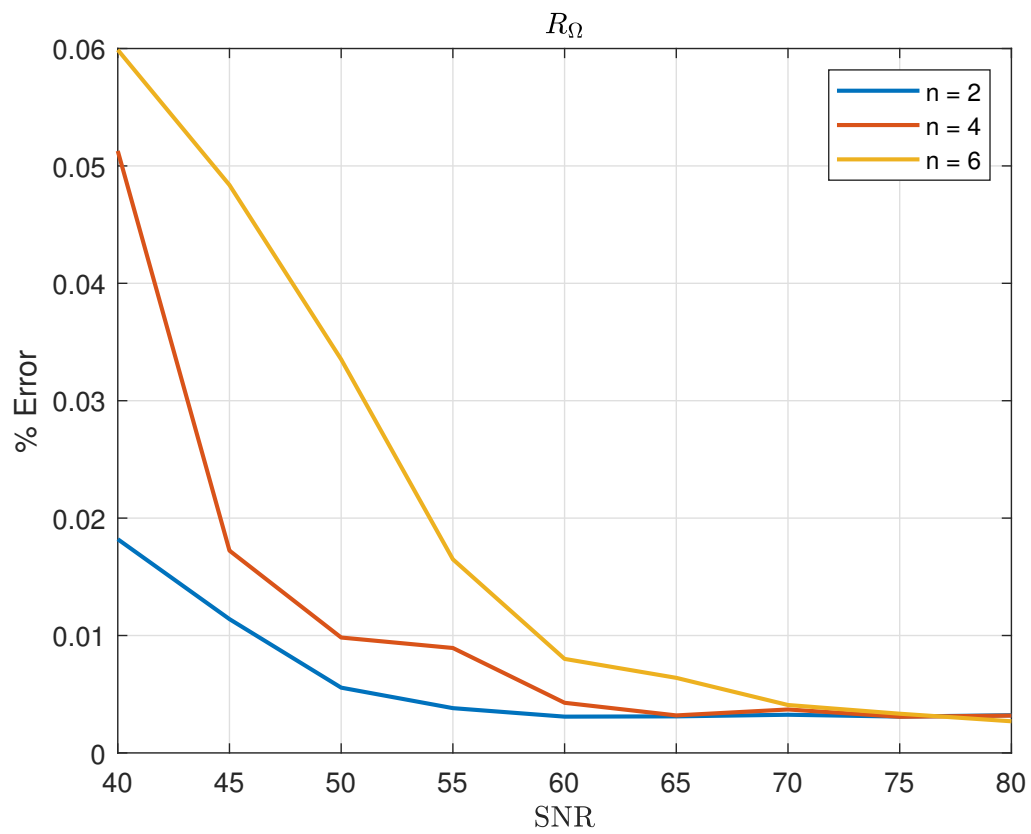


Figure 3.32: Estimated ohmic resistance for different n

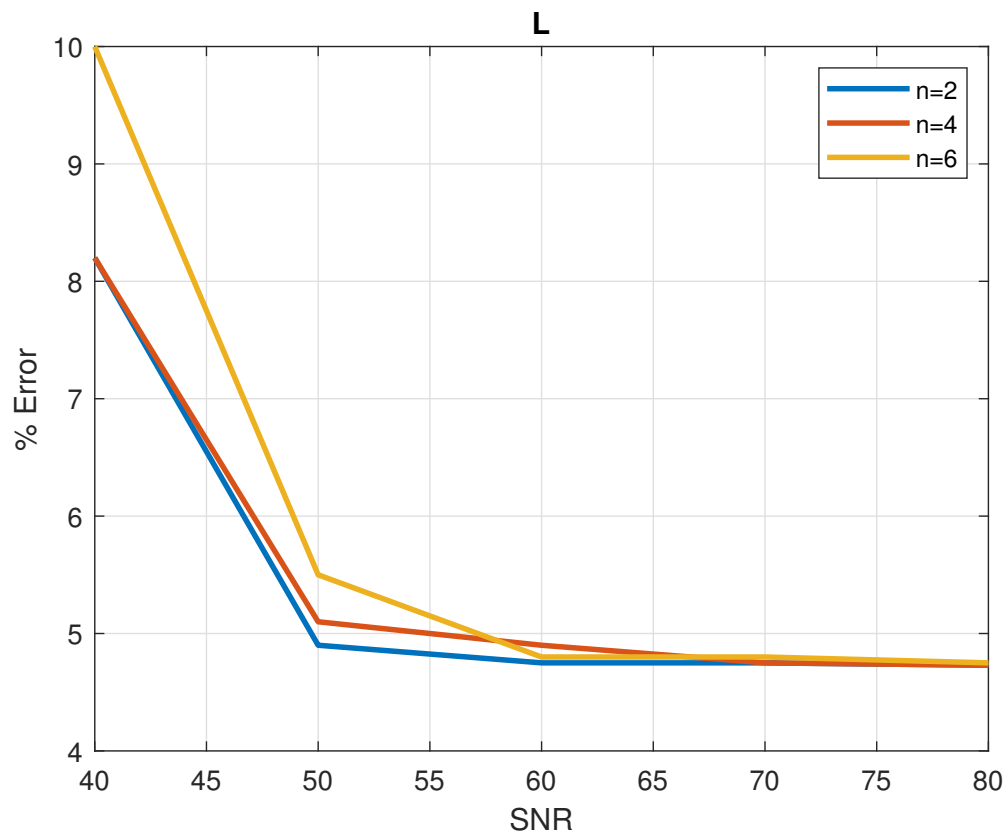


Figure 3.33: Estimated stray inductance for different n

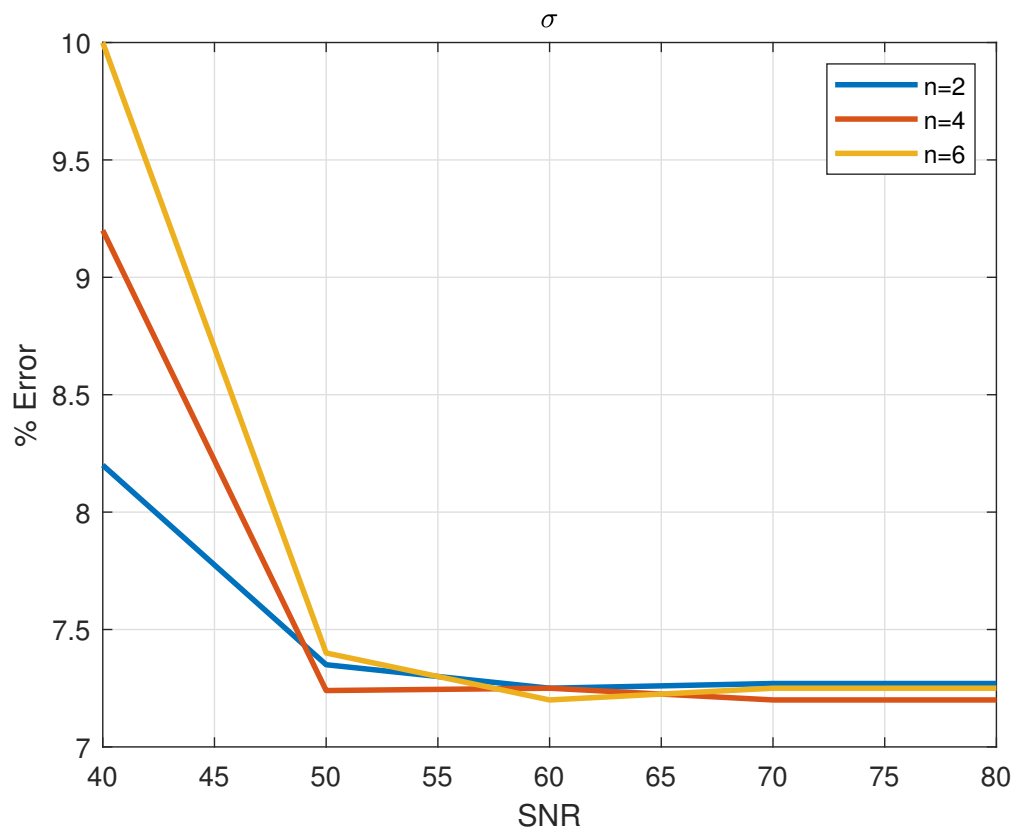


Figure 3.34: Estimated Warburg impedance for different n

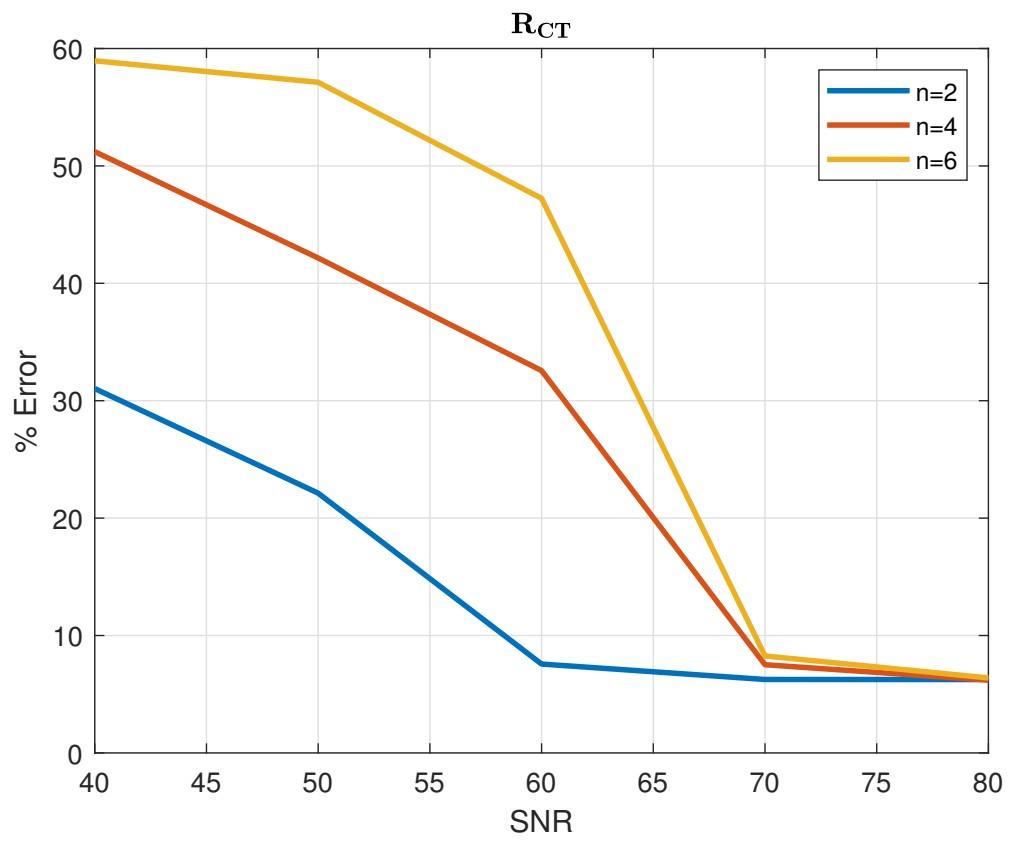


Figure 3.35: Estimated charge transfer resistance for different n

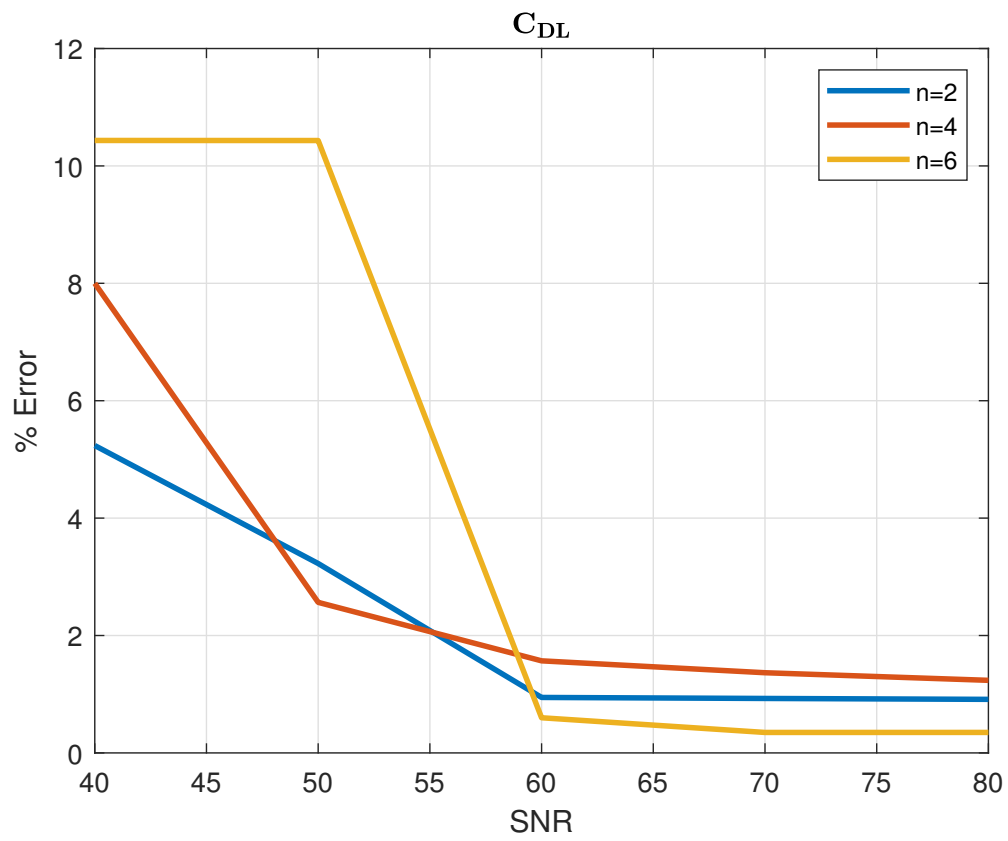


Figure 3.36: Estimated double layer capacitance for different n

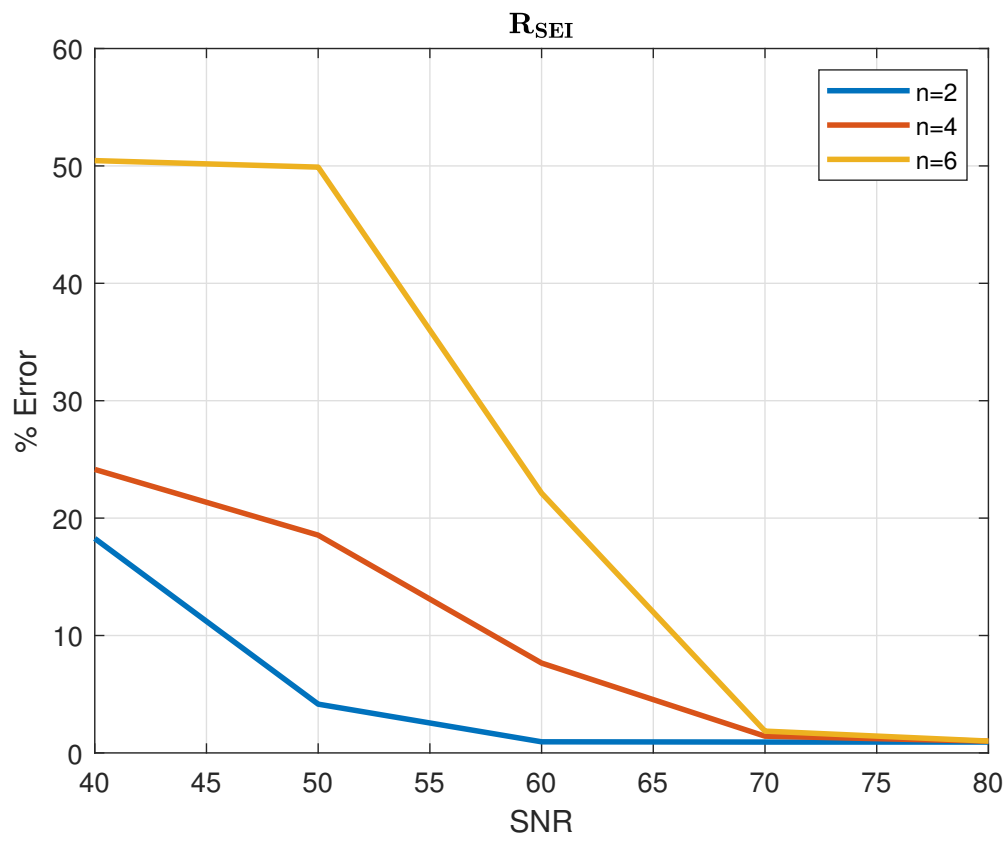


Figure 3.37: Estimated solid electrolytic interface resistance for different n

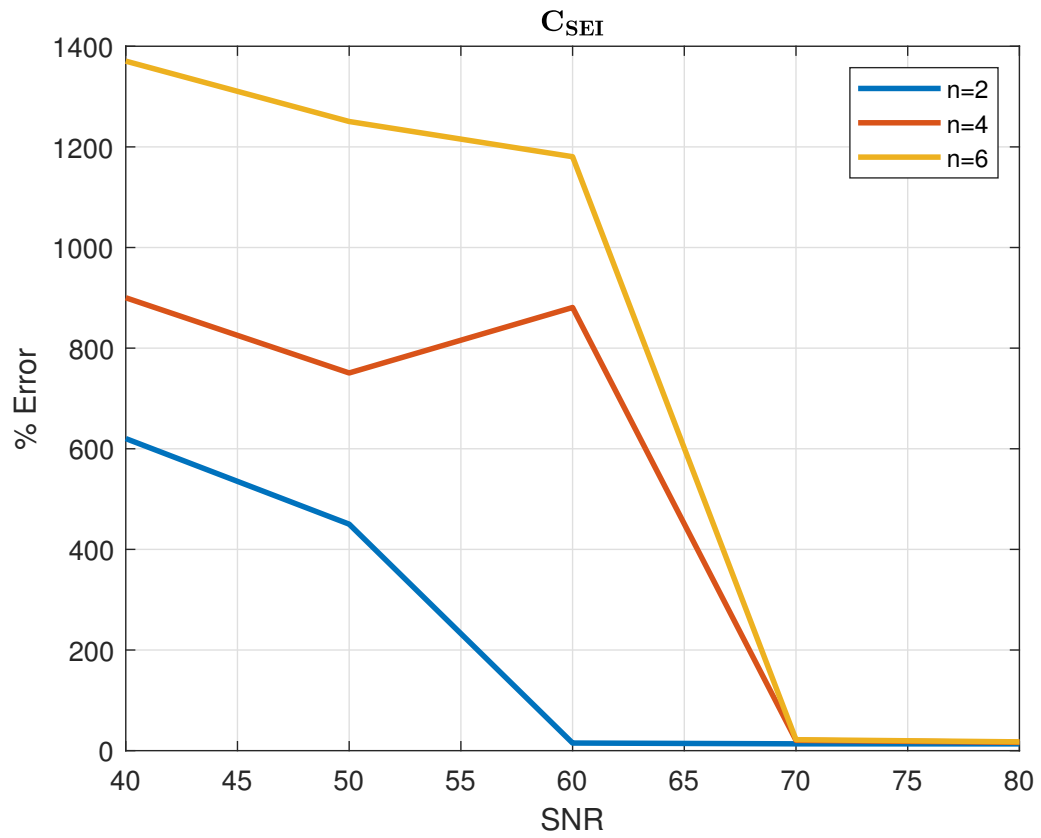


Figure 3.38: Estimated solid electrolytic interface capacitance for different n

3.6 References

- [1] J. B. Goodenough and K.-S. Park, “The li-ion rechargeable battery: a perspective,” *Journal of the American Chemical Society*, vol. 135, no. 4, pp. 1167–1176, 2013. 44
- [2] N. Hatziargyriou, H. Asano, R. Iravani, and C. Marnay, “Microgrids,” *IEEE power and energy magazine*, vol. 5, no. 4, pp. 78–94, 2007. 44
- [3] D. Cittanti, A. Ferraris, A. Airale, S. Fiorot, S. Scavuzzo, and M. Carello, “Modeling li-ion batteries for automotive application: A trade-off between accuracy and complexity,” in *2017 International Conference of Electrical and Electronic Technologies for Automotive*, pp. 1–8, IEEE, 2017. 44
- [4] A. De Vita, A. Maheshwari, M. Destro, M. Santarelli, and M. Carello, “Transient thermal analysis of a lithium-ion battery pack comparing different cooling solutions for automotive applications,” *Applied energy*, vol. 206, pp. 101–112, 2017. 44
- [5] S. Scavuzzo, R. Guerrieri, A. Ferraris, A. G. Airale, and M. Carello, “Alternative efficiency test protocol for lithium-ion battery,” in *2018 IEEE International Conference on Environment and Electrical Engineering and 2018 IEEE Industrial and Commercial Power Systems Europe (EEEIC/I&CPS Europe)*, pp. 1–5, IEEE, 2018. 44
- [6] D. Macdonald, “Electrochemical,” *Acta*, no. 51, pp. 1376–1388, 2006. 45
- [7] E. P. Randviir and C. E. Banks, “Electrochemical impedance spectroscopy: an overview of bioanalytical applications,” *Analytical methods*, vol. 5, no. 5, pp. 1098–1115, 2013. 45

- [8] G. M. Rupp, A. K. Opitz, A. Nanning, A. Limbeck, and J. Fleig, “Real-time impedance monitoring of oxygen reduction during surface modification of thin film cathodes,” *Nature materials*, vol. 16, no. 6, pp. 640–645, 2017. 45
- [9] E. Barsoukov and J. R. Macdonald, “Impedance spectroscopy theory, experiment, and,” *Applications, 2nd ed. (Hoboken, NJ: John Wiley & Sons, Inc., 2005)*, 2005. 45
- [10] A. Lasia, “Electrochemical impedance spectroscopy and its applications,” in *Modern aspects of electrochemistry*, pp. 143–248, Springer, 2002. 45
- [11] J. Song and M. Z. Bazant, “Electrochemical impedance imaging via the distribution of diffusion times,” *Physical review letters*, vol. 120, no. 11, p. 116001, 2018. 45
- [12] S. R. Islam, S.-Y. Park, and B. Balasingam, “Circuit parameters extraction algorithm for a lithium-ion battery charging system incorporated with electrochemical impedance spectroscopy,” in *2018 IEEE Applied Power Electronics Conference and Exposition (APEC)*, pp. 3353–3358, IEEE, 2018. 45, 50
- [13] W. Choi, H.-C. Shin, J. M. Kim, J.-Y. Choi, and W.-S. Yoon, “Modeling and applications of electrochemical impedance spectroscopy (eis) for lithium-ion batteries,” *Journal of Electrochemical Science and Technology*, vol. 11, no. 1, pp. 1–13, 2020. 45
- [14] H. Hosseini, D. A. Dornbusch, and G. J. Suppes, “Improved electrochemical performance of alkaline batteries using quaternary ammonia polysulfone-functionalized separators,” *Industrial & Engineering Chemistry Research*, vol. 55, no. 31, pp. 8557–8566, 2016. 45
- [15] Q.-C. Zhuang, T. Wei, L.-L. Du, Y.-L. Cui, L. Fang, and S.-G. Sun, “An electrochemical impedance spectroscopic study of the electronic and ionic transport

- properties of spinel LiMn_2O_4 ,” *The Journal of Physical Chemistry C*, vol. 114, no. 18, pp. 8614–8621, 2010. 45
- [16] B.-C. Park, H.-B. Kim, H. J. Bang, J. Prakash, and Y.-K. Sun, “Improvement of electrochemical performance of $\text{Li}[\text{Ni}_{0.8}\text{Co}_{0.15}\text{Al}_{0.05}]\text{O}_2$ cathode materials by AlF_3 coating at various temperatures,” *Industrial & engineering chemistry research*, vol. 47, no. 11, pp. 3876–3882, 2008. 45
- [17] J. Verhulst, M. Belkhat, S. Zhiyu, M. Jaksic, P. Mattavelli, and D. Boroyevich, “System and method for impedance measurement using chirp signal injection,” Apr. 11 2017. US Patent 9,618,555. 45
- [18] A. Narjiss, D. Depernet, D. Candusso, F. Gustin, and D. Hissel, “Online diagnosis of pem fuel cell,” in *2008 13th International Power Electronics and Motion Control Conference*, pp. 734–739, IEEE, 2008. 45

Chapter 4

Conclusion and Future Work

This thesis presents an analysis of electrochemical impedance spectroscopy (EIS) for battery equivalent circuit model (ECM) parameter estimation.

First, we present an improved approach for ECM parameter estimation in the frequency domain and demonstrate it using real world data. The demonstration is done using commercially available cylindrical battery cells by bringing them to various state of charge (SOC) levels. Since, it is an experimental analysis, it is hard to validate the results. Therefore, the parameters are also estimated using time domain approach at various SOC levels. The estimated parameters of the battery in the frequency domain are compared with estimated parameters in time domain. The comparison between the estimated parameters in the time domain and the frequency domain found to be very close with less than 0.01 percent error.

Moreover, time taken to obtain frequency response data of the battery is much more which restricts its use in real time applications. Therefore, we propose an approach to obtain the impedance response of a battery in reduced time. The algorithms discussed in Chapter 1 are then applied to estimate the parameters of a simulated battery. The results show that errors in the parameter estimation increase as we reduce the time taken for EIS. Therefore, errors are plotted at different signal to noise ratio for a particular time for EIS. From the results, it can be concluded that for 70 SNR,

EIS time can be reduced to approximately 150 secs.

The proposed approach in this thesis reduced the EIS experimentation time by a factor of up to 6. Consequently, it was shown that effective battery parameter estimation can be done using the proposed EIS techniques within 150 seconds. However, it was found that the proposed approach, with reduced time, is susceptible to measurement noise. As a result, the proposed approach is only suitable to high signal to noise ratio (SNR) regions. In future work, it will be beneficial to look into other, non-sinusoidal type of signals for the implementation of EIS to reduce the experimental time while maintaining their applicability in low SNR conditions. Step input is also a good signal for knowing the frequency response of the signal. Therefore, step signal can also be investigated. It is also beneficial in the future to test the proposed approach using hardware implementations so that the real world consequences of measurement noise and high sampling frequency can be further understood and quantified. For dealing with high sampling frequency PIC 32 microcontrollers or external ADCs can be investigated. Uncertainty in the measurements can also be taken into account so as to better understand the real world scenarios.

Vita Auctoris

NAME: Rohit Sengar

PLACE OF BIRTH: Haryana, India

YEAR OF BIRTH: 1998

EDUCATION: Aligarh Muslim University
Aligarh, India
2012-2015, Diploma
Mechanical Engineering

Aligarh Muslim University
Aligarh, India
2015-2019, B.Tech
Mechanical Engineering

University of Windsor,
Windsor ON, Canada
2021-2022, Master of Applied Science
Electrical Engineering